



THE HONG KONG
POLYTECHNIC UNIVERSITY

香港理工大學

Pao Yue-kong Library

包玉剛圖書館

Copyright Undertaking

This thesis is protected by copyright, with all rights reserved.

By reading and using the thesis, the reader understands and agrees to the following terms:

1. The reader will abide by the rules and legal ordinances governing copyright regarding the use of the thesis.
2. The reader will use the thesis for the purpose of research or private study only and not for distribution or further reproduction or any other purpose.
3. The reader agrees to indemnify and hold the University harmless from and against any loss, damage, cost, liability or expenses arising from copyright infringement or unauthorized usage.

IMPORTANT

If you have reasons to believe that any materials in this thesis are deemed not suitable to be distributed in this form, or a copyright owner having difficulty with the material being included in our database, please contact lbsys@polyu.edu.hk providing details. The Library will look into your claim and consider taking remedial action upon receipt of the written requests.

**MICROELECTRODE PH SENSORS BASED ON
MICROPATTERNED SILVER NANOWIRE/PAA
HYDROGEL COMPOSITE**

XIONG FENG

MPhil

The Hong Kong Polytechnic University

2019

The Hong Kong Polytechnic University
Department of Electrical Engineering

**Microelectrode pH Sensors Based on Micropatterned
Silver Nanowire/PAA Hydrogel Composite**

XIONG Feng

*A thesis submitted in partial fulfillment of the
requirements for the degree of Master of Philosophy*

November 2018

CERTIFICATE OF ORIGINALITY

I hereby declare that this thesis is my own work and that, to the best of my knowledge and belief, it reproduces no material previously published or written, nor material that has been accepted for the award of any other degree or diploma, except where due acknowledgment has been made in the text.

_____ (Signed)

_____ XIONG Feng (Name of student)

Abstract

Owing to exceptional merits such as high flexibility, lightweight, great stretchability and conformability, flexible electronics is growing towards a promising platform for personal wearable electronics, in which wearable and flexible biochemical sensors are going to be adopted to replace cumbersome and costly medical instruments for the healthcare monitoring and diagnostics. This project aims to develop a microelectrode pH biosensor to monitor ambient pH which is one of the signatures of the physiological health status in body fluids, such as sweat, tears as well as saliva.

Responsive hydrogels have become one of the essential building blocks for functional biomedical microelectromechanical system (BIOMEMS) devices for a great many biomedical applications. Here, we choose pH-responsive hydrogel, poly acrylic acid (PAA), and use an in-house optical maskless photolithography platform to photopolymerize the hydrogel to fabricate pH sensors.

Because of significant swelling in solutions with different pH values, PAA hydrogel adheres to the substrate with difficulty while it is used to make sensors working in solutions for long-term operation. To solve the problem, we developed a special stretchable microelectrode using silver nanowire (AgNW) / polydimethylsiloxane (PDMS) composite. When the

PAA hydrogel is deposited on the electrode, a diffusion layer between PAA hydrogel and PDMS can be formed to promote the adhesion of PAA. The conductivity of the electrode was optimized by the contents of AgNWs in the PDMS composite.

To fabricate microelectrode pH sensors, we mixed acrylic acid (AA) monomers with AgNWs to make pH-sensitive hydrogel composite. When such hydrogel composites are soaked into the different pH solution, the swelling of the hydrogel composite would change the spatial distribution of AgNWs in the hydrogel network and then cause the changes of composite's conductivity. With the in-house optical maskless photolithography platform, the hydrogel composite was *in situ* photopolymerized and micropatterned on the microelectrode for sensor fabrication. The effects of the microstructure on the micropatterned hydrogel composite on the performances such as response time and sensitivity of that pH sensor would be systematically researched through the measurements. Experimental results revealed that the response time of that pH sensor depend on size of microstructures. Due to the accelerated diffusion, the sensor with microstructure showed much fast response than that without microstructure. Compared with other pH sensors, the fabricated sensors showed much better performance in terms of response time.

Publications arising from the thesis

- 1 J. Wu, M. Yao, **F. Xiong**, A. P. Zhang, H.-Y. Tam, and P. K. A. Wai, "Optical Fiber-Tip Fabry–Pérot Interferometric Pressure Sensor Based on an *In Situ* μ -Printed Air Cavity," *Journal of Lightwave Technology*, vol. 36, no. 17, pp. 3618-3623, 2018.
- 2 **F. Xiong**, Y. Zhang, Ming-Jie Yin and A. P. Zhang, "Fast-response flexible microelectrode pH sensors based on micropatterned silver nanowire /poly(acrylic acid) hydrogel composite," *Sensors and Actuator B*, to be submitted.

Acknowledgments

It is necessary to publicly express my appreciation to my chief supervisor, Dr. A. Ping Zhang. Without his careful assistance on my research and life in M.Phil stage, I could not complete my research and thesis effectively. More importantly, his zeal in research inspired me to broaden insight in the research area and master more knowledge about other subjects, which are very helpful in doing my research. It is wealthy for my whole life. I would also thank Prof. Feng Yan, my co-supervisor, with his generous supports on my research and study.

I would be also grateful to those who provided significant help in finishing my experiments and the thesis. I thank to, Dr. Mingjie Yin, Dr. Jushuai Wu, Dr. Shaorui Gao, Dr. Yangxi Zhang, Dr. Jie Wang, Dr. Juncao Bian, Mr. Mian Yao, Mr. Xia Ouyang, Mr. Qi Zhang, Dr. Naixiang Wang, Mr. Yi Wang, Dr. Yuanhao Li, Dr. Qingming Chen, Dr. Feichi Zhou for their discussion and useful assistance in my experiments and thesis writing.

Last but not least, I am eternally thankful for the continuous support and love of my friends and family. It is their assistance encouraged me to finish my study, and I would really like to dedicate my thesis to them.

TABLE OF CONTENTS

	<i>page</i>
ABSTRACT.....	I
PUBLICATIONS ARISING FROM THE THESIS.....	III
ACKNOWLEDGEMENTS.....	IV
TABLE OF CONTENTS.....	V
LIST OF FIGURES.....	VII
LIST OF TABLES.....	IX
LIST OF ACRONYMS.....	X
<i>Chapter 1 Introduction.....</i>	<i>11</i>
1.1 Background.....	<i>11</i>
1.2 Research objectives	<i>13</i>
1.3 Outline of thesis.....	<i>14</i>
<i>Chapter 2 Overview of pH sensor technologies.....</i>	<i>16</i>
2.1 Introduction.....	<i>16</i>
2.2 Review of pH sensors.....	<i>18</i>
2.2.1 Conventional pH sensors.....	<i>18</i>
2.2.2 Electrical pH sensors.....	<i>21</i>
2.3 Hydrogel-based pH sensors.....	<i>26</i>
2.3.1 Properties of pH-sensitive hydrogel.....	<i>26</i>
2.3.2 Specifications of hydrogel-based pH sensors.....	<i>30</i>
2.4 Conclusion.....	<i>35</i>
<i>Chapter 3 AgNW/PDMS based electrodes for pH sensors</i>	<i>36</i>
3.1 Introduction.....	<i>36</i>
3.2 Fabrication for AgNW/PDMS electrodes.....	<i>38</i>
3.2.1 Deposition and etching method.....	<i>38</i>

3.2.2 Deposition and transfer method.....	42
3.3 Characterization of AgNW/PDMS electrodes.....	44
3.4 Conclusion.....	46
Chapter 4 pH sensors based on AgNW/PAA hydrogel composite	47
4.1 Introduction.....	47
4.2 AgNW/PAA hydrogel composite for pH sensors.....	48
4.2.1 Mechanism of AgNW/PAA hydrogel composite-based pH sensor...	48
4.2.2 Patterning and testing of AgNW/PAA hydrogel composite.....	50
4.3 Fabrication and testing of the hydrogel composite-based pH sensors.....	56
4.3.1 Fabrication of pH sensors based on AgNW/PAA hydrogel.....	56
4.3.2 Testing results.....	57
4.4 Conclusion.....	61
Chapter 5 Conclusion and future outlook.....	62
5.1 Discussion.....	62
5.2 Future outlook	63
References.....	66

List of Figures

Figure	Captions	Pages
Figure 2.1	Working mechanism of a pH Meter based on glass electrode.	19
Figure 2.2	Schematic structure of (a) a MOSFET and (b) an ISFET.	22
Figure 2.3	Electronic model of a MOSFET device.	24
Figure 2.4	Representative drawing of an interdigitated microarray electrode.	26
Figure 2.5	Acidic (\square), basic(\circ) and amphiphilic (\triangle) hydrogels being ionized through deprotonation in solutions.	28
Figure 2.6	Schematic illustration of swelling equilibrium. r_0 - initial radius, and $r_{\infty, max}$ - maximal radius.	30
Figure 2.7	a) Swelling behavior of a bulk gel, b) characteristics of a quartz crystal microbalance pH sensor.	32
Figure 3.1	Schematic illustration of AgNWs deposition on the PDMS substrate.	41
Figure 3.2	Schematic illustration of the AgNWs/PDMS electrodes fabrication with the deposition and etching method.	42
Figure 3.3	Photographs of AgNWs/PDMS electrodes during the fabrication. (a) after deposition of AgNWs; (b) after etching; (c) after stripping of photoresist.	42
Figure 3.4	Microscope picture (a) and detailed (b) picture of the surface of the AgNWs/PDMS electrodes.	43
Figure 3.5	Schematic illustration of the AgNWs/PDMS electrodes fabrication with the deposition and transferring method	44

List of figures

Figure 3.6	Photographs of AgNWs/PDMS electrodes during the fabrication process	44
Figure 3.7	Optical image (a) and laser scanning confocal microscope image (b) of AgNWs/PDMS electrodes after fabrication.	45
Figure 3.8	Optical cross-section images of fabricated AgNWs/PDMS electrodes with different concentrations of AgNW solution (a) 0.025 wt.%, (b) 0.05 wt.% and (c) 0.1 wt.%.	45
Figure 3.9	Resistance as a function of tensile for the AgNWs/PDMS electrodes	46
Figure 4.1	Schematic illustration of pH response mechanism of AgNWs/PAA composites	50
Figure 4.2	Schematic illustration of micropatterning of AgNWs/PAA composites	51
Figure 4.3	SEM images of micropatterned AgNWs/PAA composites. (a) PolyU log; (b) Clover; (c, d) Flower; (e, f) Character “Fu”. Scale bar: 100 μm .	53
Figure 4.4	SEM images of micropatterned AgNWs/PAA composites. Scale bar are 50 μm , 20 μm and 5 μm , respectively.	54
Figure 4.5	SEM images of AgNWs/PAA composites with the different concentrations of AgNWs: (a) 20wt.%, (b) 15wt.% and (c) 10wt.%. Scale bar: 10 μm .	54
Figure 4.6	Transmittance spectra of the AgNWs/PAA composites with different concentrations 10, 15 and 20 wt.%, respectively.	55
Figure 4.7	Statistics of sheet resistances and transmittances (550 nm) of the AgNWs/PAA composites with different concentrations 10, 15 and 20 wt.%, respectively.	55

Figure 4.8	Resistance responses to pH (2-7) of the AgNWs/PAA composites of different concentrations with different concentrations 10, 15 and 20 wt.%, respectively.	57
Figure 4.9	Schematic illustration (a) and cross-section (b) of an AgNWs/ hydrogel sensor integrated on a microfluidic chip.	58
Figure 4.10	Photographs of an AgNWs/ hydrogel sensor-integrated microfluidic chip	59
Figure 4.11	Dynamic measurements of 20 wt.% sensors with blank micropattern. (a) the optical image of blank pattern on microelectrode, inset is the greyscale image; (b) the dynamic response to pH changing from 2 to 7 and vice-versa; (c,d) the response curve between pH 6 and 7, 2 and 3, respectively.	60
Figure 4.12	Dynamic measurements of 20 wt.% sensors with microgrid pattern. (a) the optical image of microgrid pattern on microelectrode, inset is its greyscale image; (b) the dynamic response to pH changing from 2 to 7 and vice-versa; (c,d) the response curve between pH 6 and 7, 2 and 3, respectively.	61
Figure 4.13	Figure 4.13 Resistance changes as a function of curvature radius in pH 2 (a) and drift of the pH sensor at various pH levels (b).	62

List of Tables

Table	Captions	Pages
Table 3.1	Summarized fabrication methods of Ag NW network <i>via</i> solution processes	39
Table 3.2	Characterizations of Ag NW films with different concentration solution deposited on the petri dish.	41
Table 4.1	A comparison of pH sensor with the sensitivity response time and working rang with different sensor type.	62

List of Acronyms

Acronyms	Description
BIOMEMS	Biomedical microelectromechanical system
PAA	Poly (acrylic acid)
AA	Acrylic acid
ISFETs	Ion-selective field-effect transistors
MEMS	micro-electro-mechanical systems
Irgacure 2959	2-Hydroxy-4'-(2-hydroxyethoxy)-2-methylpropiophenone
AgNWs	Silver nanowires
CNT	Carbon nanotube
SEM	Scanning electron microscopy
DMD	Digital-micromirror device
OMSL	Optical maskless setereolithography
ITO	Indium tin oxide
PDMS	Polydimethylsiloxane
PVP	Polyvinylpyrrolidone

Chapter 1 Introduction

1.1 Background

Wearable biosensors have accepted enormous attentions by the past decades because of their immense potentialities in personal prognostics and personalized treatment [1]. Flexible and stretchable electronic devices play significant roles in individualized wearable healthcare electronics because of their exceptional properties, for instance, lower-cost, lightweight, high flexibility and satisfactory conformability [2]. Differing from the almost all of reported flexible electronics which predominantly record physical signals and activities like heart rate monitors and pedometers, the next-generation products of wearable electronics would reinforce the real-time, continuous and fast detection of approachable biochemical signals of wearers, and permits for the dynamic recording of various information about the human being's health situations [3, 4]. Particularly, the enormous capability of flexible bio-chemical sensing devices for continuously measurements about body fluid like sweat, tear and urine has not been fully realized owing to the impediments including the collection of body fluids, calibrations and dependability, and even safety issues [5].

In both chemical and biological processes, pH plays significant roles

in adjusting certain biochemical reactions. Therefore, their maintaining and monitoring would be essential and crucial in various areas diversifying from ecological science to biology and medicine technology. In biologic tissues, metabolism process can only generate while the specific biochemical conditions were met, that explains the reason why that the extracellular fluids pH would be specifically preserved approximately 7.4 through each effective organ and system. Pathology like diabetes or renal would disorder pH value of bloodstream so that the exact detection of such a parameter must be required during the therapies [6]. Even more, pH could also be detected in other body fluid. For example, the tear pH would be little acidic after wearing lenses and little alkaline over the patients suffered from keratitis. The pH of salivary would affect the dental health and could be detected in the therapeutic drug monitoring [6]. Urine pH could be the biomarker of renal disease or metabolic syndrome. Moreover, the mild acidity of sweat, ranging from 4.5-6.0, which offers effective shield from certain fungi or bacteria, is relevant to existence of lactate, and the sweat pH provides signs corresponding to body hydration levels and physical activities [3, 6].

1.2 Research objectives

This project aims at developing a microelectrode pH biosensor based on pH-responsive nanocomposites composed with hydrogel and conductive

nanowire as a chemiresistive sensor. It is expected to focus on (i) synthesis and characterization a nanowire hydrogel composite-based pH sensor; (ii) development of flexible electronic pH sensors, (iii) test and measurement in vitro using the standard buffer and pH solutions.

Feasibility of the research is supported by firm theory and previously reported work. The hydrogel that swells to respond to the varying of pH is one member from the family of stimuli-sensitive hydrogel and has been demonstrated the ability to be incorporated into micro-electro-mechanical systems (MEMS). A chemiresistive pH sensor based on a hydrogel nanocomposite deformed by pH variation when incorporated with silver nanowires will transduce the volume response of pH-sensitive hydrogel to an electrical signal. Incorporation between hydrogels and AgNWs is possible and promising for high-performance wearable pH sensor.

1.3 Outline of thesis

The thesis is mainly focused on developing a pH biosensor based on the pH-sensitive hydrogel material cooperated with 1D nanomaterial. It is structured as below. The first chapter is the general introduction for motivations for developing a microelectrode pH biosensor and goals of this thesis.

Chapter 2 introduces an overview of the pH sensor industry. This section reviews current techniques and materials for the choosing of close

collaboration for high performance pH detection methods and sensors. This chapter brings about a logical conclusion that there are several essential determinants of the pH-sensitive materials and the matrices, which have to be considered into a targeted application and finally optimizing the properties of the pH sensor.

In Chapter 3, the methodology utilized to synthesize and characterize the AgNWs/elastomer microelectrode is described. This chapter also presents some primary methods using to solve the abscission problem of sensitive hydrogel because of the swelling-shrinking degree of the hydrogel. And the necessity to understand the microscale hydrogel behavior are also discussed. Subsequently, the results for behaviors of this hydrogel are provided with detailed discussions.

Chapter 4 introduces the methodology utilized to synthesize and characterize the pH-sensitive hydrogel/AgNWs composite and also presents the working mechanism of hydrogel sensors as well as an explanation for the capability of generating swelling of the hydrogel/AgNWs composite. The experiment works with the design, packaging and measurement methods used to characterize hydrogel sensor is addressed. Results and discussions are also given.

Chapter 5 is the conclusion and future outlook of the thesis. This chapter also discusses some future work possibilities for further improvements of the hydrogel sensor.

Chapter 2 Overview of pH sensor technologies

2.1 Introduction

Detection of pH would be one of the most routine measurements in research laboratory since plenty of biological and chemical processes would be dependent on the pH value. For example,

- The measurements of pH would be significant for determining the characteristic of a matter in chemical [6]. Both biochemical reactions rate and the solubility of many biomolecules and chemicals in solution are relied on the pH value. To enhance the anticipated reaction and to avoid undesirable reactions, detection and regulation the pH of solutions count.

- The bodily fluids of biologic tissues usually have certain pH ranges. If the blood pH varies by only 0.02 pH even less, and the function of human body would be dramatically damaged [6]. The pH value of soil relates to the plants' livability, thus monitoring and controlling are necessary for farming. In addition, the polluted water from households and factories would bring about pH variations of drinking water and induce the environmental issues.

- As measurements of pH could be significant for the regulation of biochemical reactions, it would be accomplished in almost all industry processes dealing with solution: from the food or even the drinking water

to textiles, plastics, paper, semiconductors, the glass and cement.

The designation of pH comes from the grouping of p as “power” and H as the hydrogen character. The values of pH are defined with a negative and logarithmical function representing for protic activities by the equation below:

$$pH = -\log a (H_3O^+) \quad (1)$$

The pH value is adopted to state or note the extent of acidity or alkalinity of an aqueous solution. Moreover, pH value reveals the number of accessible hydrogen ions instead of the concentration of existing hydrogen ions.

This chapter mainly reviews different types of methods or materials for pH detection including the litmus paper, glass-electrode pH sensor, potentiometric pH sensors, and pH sensors based on ISFET. The pH sensors could be generally categorized into the conventional and the electrical sensors. Moreover, hydrogel-based pH sensors with their low cost and biocompatibility are also promising candidates for wearable sensors. According to the present situation over pH sensors, the hydrogel sensor would be also illustrated in this chapter with its distinctive physical background and the sensing properties for specific sensor applications.

2.2 Review of pH sensor technologies

2.2.1 Conventional pH sensors

- Litmus paper (indicators)

In the early stage, chemical indicators like litmus paper are used for measuring pH due to its color variations according to pH changes. The water-soluble lichens dyes are extracted and soaked into the paper filter stripes for producing litmus paper. And there would be two common color of litmus papers including red and blue. Red litmus paper becomes blue under basic conditions, and blue litmus paper changes into red in acidic circumstance, within the color variations happening during the 4.5–8.3 pH at 25 °C. The primary usage of a litmus paper is to detect if a solution is alkaline or acidic.

Pros & Cons: This is a rapid way to discriminate bases or acids due to its quick color change. Moreover, it is also very cheap and convenient. The shortage is that the variation of its color could not reveal the acid or alkaline degree of a solution [7].

- Glass electrode pH sensor

Glass electrode perhaps would be the most popular and pervasive commercial electrochemical sensor. Glass electrode pH sensor (Figure 2.1) is a kind of electronic device, instead of a simple electrode in the word under electrochemical sense [8]. Sensor based on glass electrode includes a bulb-like glass membrane, that provides the name and a tubular body with electrically insulation, which divides a silver/silver chloride electrode and

an inside referencing liquid from the target solution. The electrode of Ag/AgCl is adopted to connected with a lead cable which is terminated with certain connectors which would wire up to a specific voltmeter instrument, as the pH meter [8]. The glass electrode pH meter would gauge the differential voltage and the variations through the bulb-like glass membrane. The differential potentials would be acquired from two local parts. One is that the glass indicator electrode which is faced with the internal solution, and the other point is realized by the connection with the calomel reference electrode, soaked in a target solution.

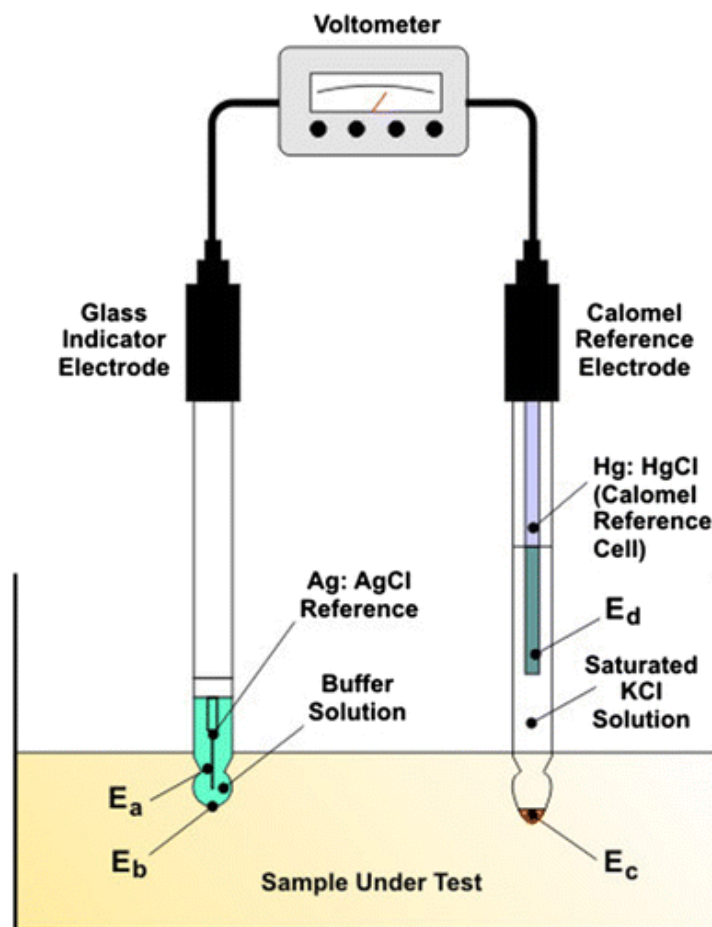


Figure 2.1 Working mechanism of a pH meter based on glass electrode [8].

The replacement of the hydronium ion (written as a proton, H^+) around the glass membrane and the adjacent target-solution, and the balance process of this replacement, would be the crucial mechanism of H^+ sensing. Within whichever interface dividing two individual parts whose exchange balance of ions is instituted, the solid membrane/target solution boundary turns out to be the spot of a differential potential. This glass solid membrane possesses two boundary/solution surfaces, and there would be a potential accumulation on each of them within conflicting polarization. However, the pH surrounded by the membrane with bulb-like structure would be steady since the solution inside is impenetrable. Thus, the internal interface potential is stabilized, appending simply as the offset of the whole voltage of the pH sensor device. The supplementary function to this compensation originates from a potential of the internal electrode immersed in solution, and for the reference electrode, that would be also stabilized. The potential variations in the pH sensing electronics are consequently because of the pH alterations of the target solution and differential voltage formula among glass electrode and referencing electrode structure is

$$E_{GE} = E' + RT/2.303F \log a (H_3O^+) \quad (2)$$

Where an (H_3O^+) denotes the hydronium activity; F represents the Faraday coefficient, 96,485.3 C, 2.303 is the conversion constant of natural and common logarithm; T represents the kelvins temperature; R

denotes the coefficient of molar gas around 8.31 J/mol K ; E' equals the quantity of the compensation potentials coefficient of the internal glass membrane surface/target solution [9]. For each one unit of pH, the value of $RT/2.303F$ is around 0.060 V nearby 30°C .

Pros & Cons: Even though the glass electrode pH sensor presents rapid, precise and dependable readout, it would suffer from shortages such as brittle materials and sophisticated framework. Therefore, it could not be applied in the wearable healthcare area.

2.2.2 Electrical pH sensors

- pH sensor based on ion sensitive field effect transistor

ISFET would be the alternative to glass electrode, which applies pioneering MEMS technologies. The ISFET is a kind of offshoot of a classical electronic module named as metal oxide silicon field effect transistor (MOSFET), that comprises the semiconductor substrate within source and drain electrode connections, seeing in Figure 2.2. A silicon electrical insulator is overlaid on the substrate between the two electrical contacts, which itself is also coated with a gate electrode. If applying a potential on the gate electrode of that transistor, and the caused variations of electrical field free the source and drain current flows. Considering as the ISFET, the dielectric layer directly contacted to target solutions would be tested. After the choice with a satisfactory dielectric layer, such as SiN_x or alumina,

proton would pin to the interface on the dielectric layer consistent with the pH value of target solution. An electric field would be induced by those positives, which could regulate the drain/ source currents. For quantifying that phenomenon, the source/gate potential is detected which would be employed through referencing electrode to uphold the source/ drain current within steady values. Value of pH could next be exported with relatively high accuracy.

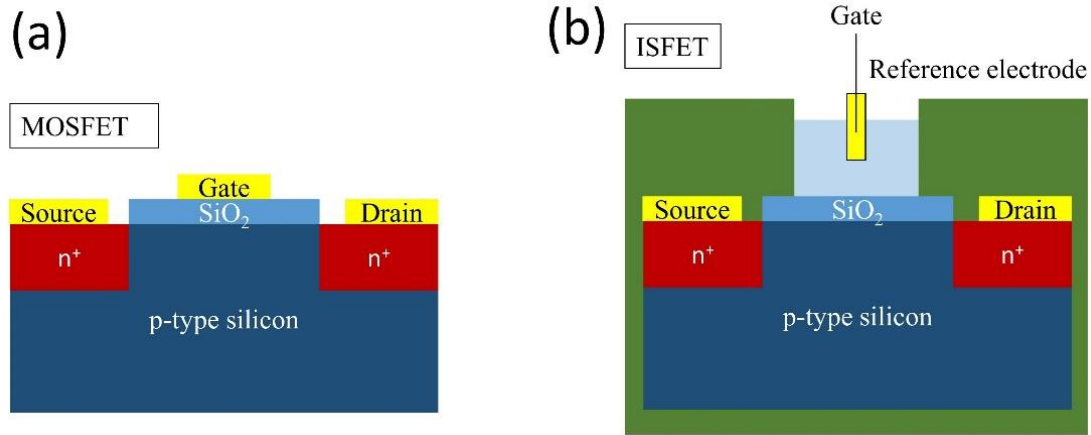


Figure 2.2 Schematic structure of (a) a MOSFET and (b) an ISFET.

The MOSFET model would be a significant bases to comprehend working principle of ISFET. Paralleled with MOSFET, the calculation of the threshold voltage, $V_{TH(MO)}$, is expressed within the gate potential value (V_G) which would be essential to induce interface reversal known as

$$V_{TH(MO)} = \Phi_M - \Phi_{Si} - \frac{Q_{ox} + Q_{ss} + Q_b}{C_{ox}} + 2\Phi_f \quad (3)$$

where, Φ_f = the semiconductor Fermi potential, Q_b = exhaustion charges of semiconductor per elemental area, Φ_M is the gate metal's work

functions, Φ_{Si} equals the bulk semiconductor's work functions, Φ_{MS} is the differential work function between metal and semiconductor, Q_{ss} equals the interface pinned-state charge in every elemental area in the surface between insulator and semiconductor, C_{ox} represents capacitance in every elemental area of the dielectric layer, Q_{ox} is depletion charges in dielectric layer [9,10].

As for ISFET, due to similar manufacturing procedures, causing the same identical substantial parts with same threshold potentials. However, with the inducement of the solution among reference and insulator, two more voltages would be created: the consistent voltage of reference, E_{ref} , and external voltage $\Psi_0 + \chi^{sol}$ in insulator / electrolyte surface, where the surface potential is represented as Ψ_0 , as function of the solution pH and the surface dipole potential of the solvent is shown as χ^{sol} , having a consistent amount. The equation for the threshold voltage of ISFET consequently is shown below:

$$V_{TH(IS)} = E_{ref} - \Psi_0 + \chi^{sol} - \Phi_{Si} - \frac{Q_{ox} + Q_{ss} + Q_b}{C_{ox}} + 2\Phi_f \quad (4)$$

Similar with MOSFET, the source/drain currents in ISFET have the common formulas in saturated or non-saturated mode could be straight represented as below respectively:

$$I_{DS} = C_{ox}\mu \frac{w}{l} \left[(V_{GS} - V_{TH(IS)})V_{DS} - \frac{1}{2}V_{DS}^2 \right] \quad (5)$$

$$I_{DS} = \frac{1}{2}C_{ox}\mu \frac{w}{l} (V_{GS} - V_{TH(IS)})^2 \quad (6)$$

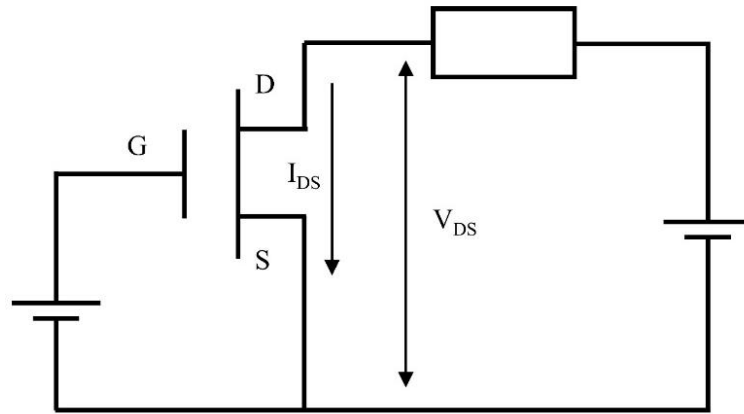


Figure 2.3 Electronic model of a MOSFET device.

Where electron mobility is shown as μ , w represents the channel width, l is the channel length, V_{GS} represents voltage between source and gate in volts, V_{DS} is the voltage between source and drain. A fictitious constant is shown as literals $C_{ox}\mu\frac{w}{l}$, and V_{DS} would be consistent after employing a voltage. However, the factor V_{TH} could be regulated chemically through the surficial voltage between insulator and electrolyte surface. Ψ_0 , the interfacial potential can be shown as a function of pH of the solution. ISFET is, therefore, an ion sensing device, i.e., an ion sensor. In ISFET, therefore, the I_{DS} / V_{DS} output curves are recorded as a function of pH of the solution [9,10].

Pros & Cons: pH sensors based on ISFET have a minor dimension because of the newest production technology and possess a shape with the magnifying system for measurement. ISFET would be relatively costless matched to the electrode in glass type. Shortages accompanied that kind of pH sensor would be the response wandering during the long term, that

would consequently cause the decrease of sensitivity and accuracy.

- Potentiometric pH sensor

The signals of potentiometric pH sensors would be measured within differential potentials (voltages) among the reference and working electrode. The working electrode's voltage would be reliant on the contents of a target chemicals inside an aqueous liquid, and the reference voltage would be delivered by the reference electrode. For the clinical applications, biological or dermatological purposes, like assessments of linear poly-propylenimine or poly-ethyleneimine (two kinds of enzymes) would be produced through three monomers' polymerization including diethylenetriamines, 1,3-diaminopropanes and ethylenediamines. Those materials would be appropriate for pH sensing due to their excellent biochemical affinities to interfaces of electrode in electro-polymerization process [11]. Electro-synthesized poly-pyrrole was applied into the miniature potentiometric pH sensors. This kind of pH sensor has interdigitated microelectrodes in which the sensing electrode would be covered with a thin film of poly-pyrrole, and the other electrode would be coated with silver layer as reference electrode, which is schematically shown in Figure 2.9 [11].

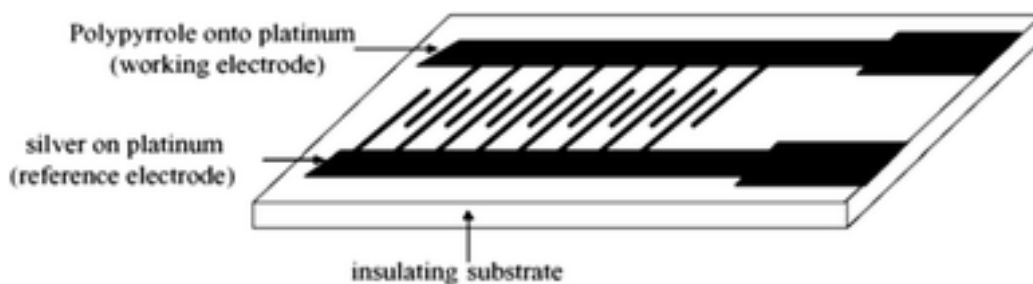


Figure 2.4 Representative drawing of an interdigitated microarray electrode [11].

Pros & Cons: Potentiometric pH sensor has rapid responses and would be capable within severe condition including high temperature or pressure. It could be utilized commonly because of the good repeatability during the measurement of from pH 0 to 14.

Long-established glass electrodes have been produced and employed extensively, however, they have some disadvantages for wearable applications. The structure of glass type sensors possess impediment to be utilized for *in vivo* biomedical and clinical monitoring application because of the brittleness of glass, limited size and insufficient deformability. To realize small size and firm configuration, ion-selective field-effect transistors (ISFETs) pH sensors, solid-state pH sensors and hydrogel pH sensors have been proposed [7-15]. The pH sensors ISFET have the power consumption concerns because of the requirement of FET operation. The pH sensors with hydrogel film utilize the physicochemical characteristics of the pH-responding swelling/deswelling polymers for detection of the mechanical deformation induced electrical resistance changes.

2.3 Hydrogel-based pH sensors

2.3.1 Properties of pH-sensitive hydrogel

Sensitive hydrogels are three-dimensional network polymers cross-linked with molecule chains. They could be synthesized through cross-linking process with polymer monomer, that would be instantaneously synthesized into chains and linked together at the same time. Because of the interactions among these hydrogel chains, the cross-linked hydrogels could be indissoluble but swell with the absorption of solution.

Polyelectrolyte hydrogels consist of weakly acidic or basic groups which could be ionized during the crosslinking process. Thus, these ionized groups density inside the net dramatically enlarges along with a sufficient production of free counter charges internal hydrogels, that would induce the status alteration within electrostatic repulsion. The diminution of the charges' densities even the concentrations of free counter ions inside gels causes shrinking. If these ionizations were finished, the transformation procedure would stop. [12] The osmotic pressure would be declined and the gel would be shrunk (seen in Figure 2.5). The figure reveals three common hydrogels' volume transformation.

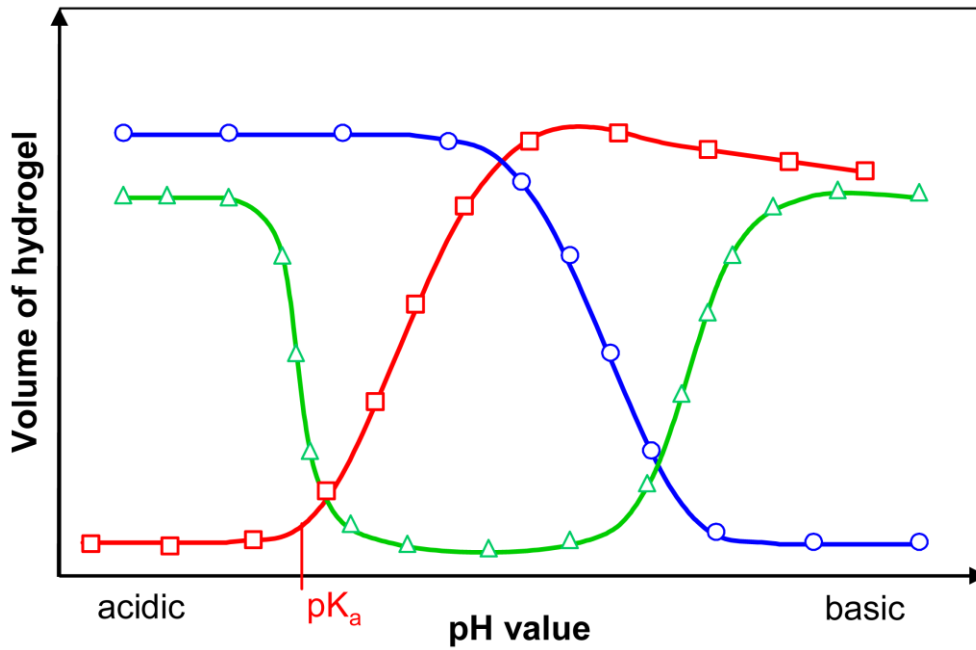


Figure 2.5 Acidic (\square), basic(\circ) and amphiphilic (\triangle) hydrogels being ionized through deprotonations in solution [14].

Hydrogels' electrostatic interconnection to the osmolality equilibrium would be recognized within the spread-out strain $\Delta\pi_{ion}$ so that there would be

$$\Delta\pi = \Delta\pi_{elast} + \Delta\pi_{mix} + \Delta\pi_{ion} = 0. \quad (7)$$

The counterions' movement inside hydrogel would be rapid as possible for ensuring their liberation to the nearby liquid. Since these gels would hold the neutral nature of charges, they could only replace them within some ions from nearby solutions instead of liberating their counterions [13,14]. Such kind of replacement could be involved with the osmolality equilibrium of hydrogels and the nearby solution causing the swelling degree changes. Within the weak ionic strength, the replacements of ion would be fringe, and thus the effects on the transformation would be

insignificant. By amplifying the concentration of nearby ions, the active counterions replacements inside hydrogels and the arise of osmolality in gels would be effectively achieved. The above state would be related to the swelling process. These donation from the strengths of ions $\Delta\pi_{\text{bath}}$ to would be deliberated:

$$\Delta\pi = \Delta\pi_{\text{elast}} + \Delta\pi_{\text{mix}} + \Delta\pi_{\text{ion}} + \Delta\pi_{\text{bath}} = 0. \quad (8)$$

Hydrogels' swelling/deswelling processes would demand a time-consuming transportation of ions and solvents. Two transporting principles should be recognized to originate the transitions fo volume stage. The originating incentives should be transferred inside gels firstly, for example, pH difference and differential temperature, which would be interconnected within the osmolality equilibriums' variations. Transportation would happen either energetically through thermal transferring (named as the coefficient of transferring heat, D_T) or through the dispersion fo liquids into gels (named as the coefficient of spontaneously transferring, D_S) shown as Figure 2.6. As the second principle, to acquire the transformation balance from varied osmolality equilibriums, hydrogels swell/ shrink through saturating/ liberating the solvent. Therefore, hydrogel network's chains should be transferred for ensuring their novel locations. Consisting of the soluble agent dispersion and the movement of network chains, TANAKA and FILLMORE proposed a novel model for the cooperative dispersion described as the coefficient of cooperative dispersion, D_{coop} .

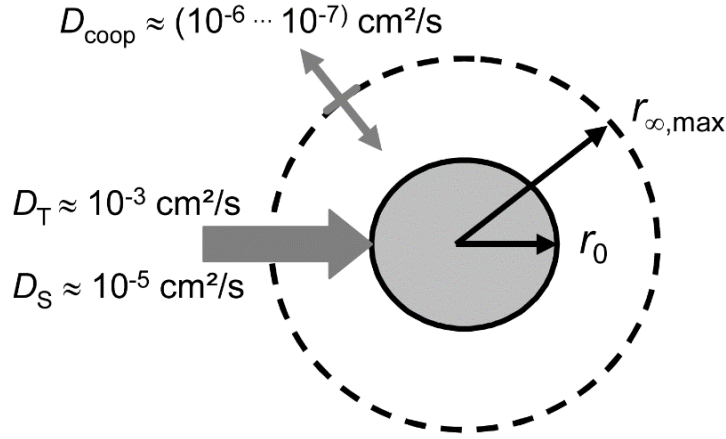


Figure 2.6 Schematic illustration of swelling equilibrium. r_0 - initial radius, and $r_{\infty, max}$ - maximal radius [14].

Within spherical hydrogels, as presented at Figure 2.6, the mechanism forecasts the time quantity about the transformation process as below:

$$\tau = r^2 D_{Coop} \quad (9)$$

where r represents the ending semidiameter. The hydrogel's semidiameter in the swelling procedure has to be presented as below

$$r(t) = r_0 + (r_{\infty, max} - r_0) \cdot (1 - e^{-t/\tau}) \quad (10)$$

and for the procedure of deswelling

$$r(t) = r_0 + (r_{\infty, max} - r_0) \cdot e^{-t/\tau} \quad (11)$$

Summarized equations from 9 to 11, for acquiring tiny time quantities the hydrogel's dimensions must be tiny enough because of the dependency in square. [14] Furthermore, the hydrogel's time quantities could increase according to the capacity of buffers.

Poly(acrylic acid) has drawn great attentions because of the better biocompatibility and outstanding thin-film machinability among diverse hydrogels. In addition, it would be more suitable to form bio-functional

surfaces because of abundant contents of carboxylic acids for modifying physically and chemically. Therefore, PAA would be promising to be employed in emergent areas, like biosensors or biomedical electronics.

2.3.2 Specifications of hydrogel-based pH sensor

- Measurement's sensitivity

Most hydrogel-based pH sensors would operate in the range of state alteration. For poly (vinyl alcohol)-poly (acrylic acid), its span would be ranged from the pH 4.7 and pH 9 since the ionization procedures are completed while pH 9, as shown in Figure 2.7a. The rapid variation of hydrogel's volume in the state alteration range would cause the special sensitivity, in orders of 10^{-3} to 10^{-5} per pH unit. Figure 2.7b shows that the response of this pH sensor would be roughly linear in this span. Measurements of pH beyond this state alteration span should be deprecated. Beneath that span, hydrogels would be shrunken associated with poor sensitivities. Above this span, hydrogels would be swollen with decreased sensitivities and noteworthy effects from the solution's ionic strengths, as presented in Figure 2.7a. [15] The sensor sensitivity here is (13.2 ± 0.62) kHz/pH in pH span ranged from 2.55 to 3.45.

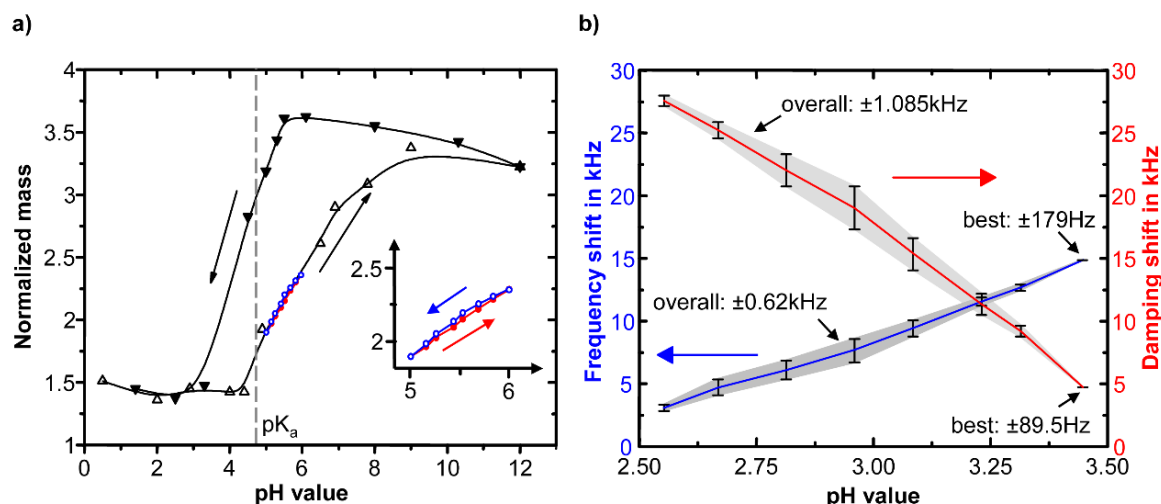


Figure 2.7 a) Swelling behavior of a bulk gel, b) characteristics of a quartz crystal microbalance pH sensor [15].

● Measurement's accuracy

The most sensors' measuring accuracy would be identical with a 95 % confidence's standard deviation. Common reasons for this opposing influence would be intricate incidents inducing the distinctive hysteretic actions presented at Figure 2.7a. The typical acidic to the basic curves would be entirely dissimilar with the basic to acidic curves. Hydrogels' mechanical and optical properties are reflected in these phenomena. SUZUKI illuminates that incident of the counterion substitution by the suitable ions like sodium ion and the overload of these ions at the internal of hydrogels would cause the shielding of the ionized groups [15].

The retardation could be enormously decreased due to the strong restraint from operating span during the range of state transition, as presented at inset of Figure 2.7a. For example, the operating span of the

sensor based on crystalline silica (Figure 2.7b) ranges pH 0.9 associated with a generally accuracy around 1.09 kHz for damped deviation.

As indicated before, the sensitivity of pH sensors would be affected through decreasing variations of hydrogel volumes. These results from the pH sensor additionally point to the diminish in accuracy of measurements.

- Working range

The pH sensor's working span could be expressed through the hydrogel constituent's collection. For example, the operating spans are completely associated with ionizable group's pKa. The wholesale hydrogel exhibits obvious pKa around 5, that deeply concurs with PAA's pKa, as shown in Figure 2.7. However, for exceptional situations, the hydrogel sensors' pKa would be deviated as presented in Figure 2.7b as an instance with the hydrogel-based crystalline silica pH sensor with 2.2 pKa. Reasons of this deviation would be the reliance of the condition of stage transition over the hydrogel layer's thickness.

- Response time

The pH sensor's response time would be reliant on the featured dimensions of hydrogel. Around upper millisecond responses of a pH sensor would be acquired with hydrogel typical sizes in nanometer span, meanwhile, several minutes responses would be achieved in the sizes around hundreds of microns [16].

The ionizable strength effects above response time could be tested on pH sensors within same thicknesses. The hydrogel-based crystalline silica pH sensor has been researched in acidic span within great ionizable strengths and achieved response time less than five hundred milliseconds. On the other hand, the sensor operating over unbiased pH span within low ionizable strengths has response time around eighty seconds [17].

In addition, the pH sensor's response time would be deeply involved with osmolality equilibriums that affect the hydrogel's transferring procedure. pH sensor with hydrogel's mechanical properties would incline to exhibit giant variations of swelling/deswelling time. For curved plate sensors, the dish would restrain degrees of swelling because of resilient counterforces inducing around 8 hours response time [18]. The contrary deswelling procedure would be under promotion of resilient strains of the curved dish for the forty minutes of response.

On the contrary, there would be no giant differences of swelling/deswelling time with the unrestrained hydrogels. For instance, crystalline silica pH sensors hold response time around five hundred milliseconds in swelling and eight hundred milliseconds in deswelling [19].

- Calibration and offset correction

Sensors excellent linearity during their operating span would permit purposes for straightforward calibrations. It is worthy to be mentioned that

corrections should be operated alone within each procedure.

Excepted with sensor's calibrations, offsets could be rectified through regulating the purpose-inducing dimensions, for instance, the dish distance to hydrogels. The essential mechanism of these mechanical regulations would be expressed. With certain hydrogels holding dual sensitivities, the offset's amendments could be operated in electric.

- Long-term stability

Within operating process in the first, the hydrogels-based pH sensors would exhibit an inferior accuracy. The variations in hydrogel network's structures would cause this consequence since there are too short chains to be disconnected and other strings to be arranged optimally. Working through numerous rounds, these hydrogel networks would be built up to increase the accuracy of measurement.

A significant issue would be hydrogel layer's abscissions during sensing process. The obstacle could be evaded through applying the adhesive agent, thin hydrogels, film-developed hydrogels or enclosing of hydrogels' elements.

Within target liquid of intensive ionizable strengths, barely solvable salt could be accrued internal of hydrogels that would cause irreparable failures [20]. There would be certainly developed agglomerates within several hours. And the hydrogel's thin film would barely incline that

phenomena. For evading such consequences, pH sensors should be consistently cleansed and kept in deionized solutions.

2.4 Conclusion

In this chapter, approximately various pH sensors with different mechanism and distinct chemical properties for diverse materials has been discussed. This review would provide principal grasps about the mechanisms of various kinds of pH sensors. Moreover, for pH sensitive hydrogels, they exhibit ultrahigh sensitivities over span around 10^{-5} per pH. Their demonstrated measurements' accuracies were ranged from 10^{-2} to 10^{-3} on average. Although these technologies based on hydrogels could not give entire electronics working in the wide pH spans, the benefit of these technologies would be enormous variety within suitable hydrogel films presenting adapted sensing solutions for numerous specialized purposes. In addition, pH sensors with hydrogels could be miniaturized and would be combined within MEMS technologies. Their fabrications could be achieved through sophisticated transducing mechanisms. These excellent performances make them candidates for wearable pH sensing device.

Chapter 3 Flexible transparent electrodes based on AgNWs/PDMS for pH sensor

3.1 Introduction

Over the last decades, intelligent electronics adjacent with Internet would permit massive information conversation within excellent speed. However, existing intelligent electronics would be almost inflexible since their fabrication with traditional MEMS procedure utilizing silicon wafer, rigid circuits, or other inflexible materials [21-23]. On the contrary, the next-generation developments of intelligent electronics anticipated light-weight devices within minimal spending of energy in flexible forms which could be directly adjacent with human body. Therefore, the basic requirements of the wearable electronics should be comfortable and safe as well as easy to use and to wear.

Since conventional fabrication processes of electronic devices commonly require harsh environments including high-temperature and high-vacuum, and that is difficult to operate in a flexible podium with low-temperatures and excellent compatibilities. Fortunately, several inimitable features from nanomaterials such as ultrahigh ratio of surface to volume and minimal process temperatures could satiate these requirements. For particular, nanomaterial could be sorted as 1-dimensional (1D) nanowires,

2-dimensional (2D) nanoscale thin-films, and 3-dimensional (3D) nanostructures [24-29]. Because of the greater aspect ratio of the 1D nanomaterials geometry, they exhibit excellent optical transparencies and meanwhile good electrical properties. Therefore, 1D nanomaterials would be broadly recognized as candidates for applied translucent wearable purposes.

Within diverse 1D nanomaterials, Ag NWs has accepted outstanding focuses from numerous scientists to replace indium tin oxide (ITO) because of their outstanding conductivities and good optical transparencies. Moreover, Ag NW would be a noble metal; it presents great mechanical properties meanwhile excellent chemical stability in harsh states and outstanding thermal conductivity for flexible electronics. Therefore, we adopted Ag NWs as the conductive material for the flexible pH sensor.

In this chapter, we present a simple procedure to fabricate Ag NW electrodes on transparent crosslinked PDMS substrates with a smooth electrode surface. The resulting Ag NW/elastomer electrodes have high transparency and relative low sheet resistance. The electrode is suitable for the fabrication of flexible/wearable pH sensors. Furthermore, elastomer substrate provides a flexible interface to fit the swelling of sensing film as well as intersectional polymer-work as the enhancement for adherence of sensing film.

3.2 Fabrication for AgNW/PDMS microelectrodes

Basically, flexible electrodes with high transparency based on AgNW for wearable electronic purposes would utilize percolating networks of Ag NW structure that enables outstanding electrical, optical and mechanical properties together. For making a flexible electrode of an Ag NW network by solution processes, several deposition routes of Ag NW network are discussed and summarized in Table 1 [30-39].

Table 3.1 Summarized fabrication methods of Ag NW network *via* solution processes

Process	Dimensions of Ag NW (diameter, length)	Transmittance at 550 nm (%)	Sheet resistance (Ω/sq)	Substrate material	Ref.
Drop casting	D: 70 nm; L: 8 μm	80.6	9.3	PET	[30]
	D: 60 nm; L: 4-10 μm	~80	10	PMA	[31]
	D: 60 nm; L: 6 μm	90	100	PAA	[32]
Spray coating	D: 115 nm; L: 30 μm	85	10.76	Glass	[33]
	D: 50 nm; L: 5-10 μm	80	13 \pm 2	PET	[34]
Mayer-rod	D: 223 nm; L: 143 μm	91	13	PET	[35]
	D: 90 nm; L: 50 μm	85	25	PEN	[36]
Vacuum filtration	D: 84 nm; L: 6.6 μm	92	100	PET	[37]
	D: 160 nm; L: 95 μm	89	9	Glass	[38]
Printing	D: 56.6nm; L: 8.63 μm	87.2	46.1	PET	[39]

No single Ag NW network fabricating techniques could satiate all purposes for diverse appliances. Vacuum filtration can fabricate a uniform thin-film in the early stage of research with Ag NW. Nevertheless, considered with that the transferred fields would be utterly reliant on the dimensions of filters, this procedure may neglect transformation in large

area. As the replacement, diverse straight print techniques like spray-coating and other drop-on-demand technologies have been presented to resolve this giant field problems. Nevertheless, procedures mentioned above would also present unsuitable throughput capacities for massive productions, and experimental conditions would restrict properties of transferring Ag NW network [40]. Thus, there should be great efforts to improve relative technologies.

3.2.1 Deposition and etching method

We adopted the drop-casting method to fabricate the Ag NW/PDMS electrode. The drop-casting process as schematically illustrated in Figure 3.1. A PDMS substrate prepared on glass was introduced by spin-coating and thermo-crosslinking the elastomer kit SYLGARD 184 (w/w = 1:10) from Dow Corning, USA. Then Ag NW dispersion in IPA was drop-cast to form conductive Ag NW thin film on a prepared PDMS substrate within a 35mm petri dish (around 2ml volume). With the evaporating of IPA at room temperature in the fuming hood, the Ag NW conductive network on PDMS substrate could be formed in 2 hours. And then, the resulting film was heated in an oven at 80°C for 30 min to remove polyvinylpyrrolidone (PVP) capping layer which is the byproduct during the AgNW fabrication process to improve its conductivity.

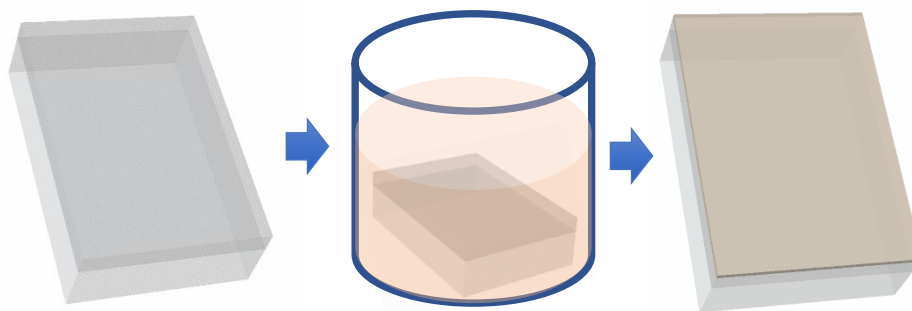


Figure 3.1 Schematic illustration of AgNWs deposition on PDMS substrate.

The Ag NWs employed above have an average diameter of approximately 60 nm and an average length of about 40 μm . Since the volume of the Ag NW dispersion was immovable, the sheet resistance of the conductive film on PDMS could be controlled by changing the concentration of drop-cast Ag NW solution. Table 2 shows the data and the relationship between the concentration of drop-cast Ag NW solution and the thickness as well as sheet-resistance of Ag NW conductive network on PDMS substrate.

Table 3.2 Characterizations of Ag NW films with different concentration solution deposited on the petri dish.

In 35mm petri dish (~2ml)	Concentration	Thickness	Sheet resistance
	0.1 wt.%	$\sim 6 \mu\text{m}$	0.6 $\Omega/\text{sq.}$
	0.05 wt.%	$\sim 2 \mu\text{m}$	1.6 $\Omega/\text{sq.}$
	0.025 wt.%	$\sim 1 \mu\text{m}$	4.6 $\Omega/\text{sq.}$
	0.01 wt.%	$\ll 1 \mu\text{m}$	10~100 $\Omega/\text{sq.}$

As illustrated in Figure 3.2, we fabricated the Ag NW-based electrodes on the PDMS substrate by adopting the maskless

photolithography to form the barriers for Ag NW patterning, after which the Ag NWs were etched away by an acidic solution, followed by stripping of the photoresist (AZ4620, Merck, Germany).

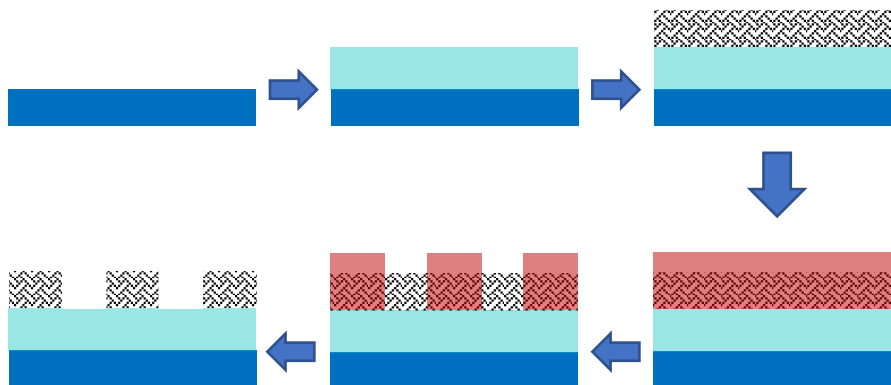


Figure 3.2 Schematic illustration of the fabrication process of the AgNWs/PDMS electrodes by deposition and etching method

After removal of the remaining photoresist, we can get a pair of electrodes based on AgNWs (seeing in Figure 3.3).

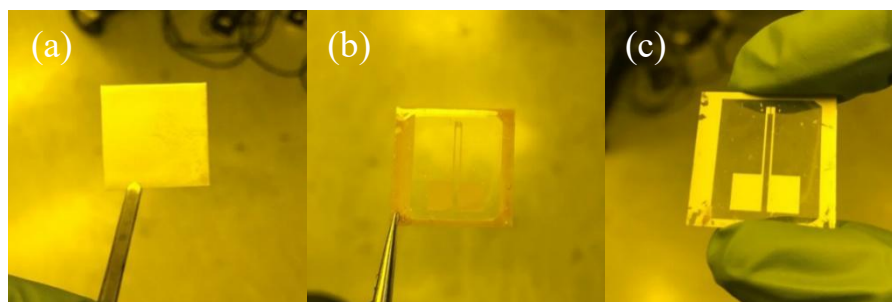


Figure 3.3 Photographs of AgNWs/PDMS electrodes during the fabrication. (a) after deposition of AgNWs; (b) after etching; (c) after stripping of photoresist.

However, in this trial experiments, we found that the Ag NWs naturally deposited on the PDMS substrate have inherent disadvantages like weak adherence and fragileness (the right image of Figure 3.3). Also,

at the view of the microscope, we found there are not only soiled in the electrode pad but also unknown residues in the etched area (seeing in Figure 3.4).

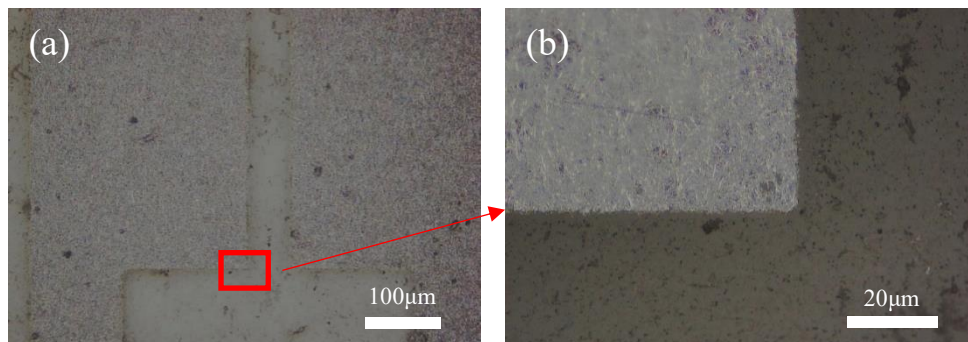


Figure 3.4 Microscope picture (a) and detailed (b) picture of the surface of the AgNWs/PDMS electrodes.

Therefore, due to the reasons aforementioned, we adopted another kind of fabrication process to get a clean and robust AgNWs PDMS electrodes.

3.2.2 Deposition and transfer method

The procedures for fabricating AgNWs/PDMS flexible electrodes are schematically shown in the Figure 3.5. Similarly, AgNWs solutions would be drop-casted over the clean silicon. AgNWs suspensions are then dehydrated for forming a homogeneously conductive AgNWs network within thin thickness ranging around several microns. Then, the liquid silicone would be cast over the AgNWs network, followed by curing at 65 °C for 12 h. When peeled off the substrate, the AgNWs film is bonded to the cured PDMS. The AgNWs film is buried just below the PDMS surface (i.e., the top surface is a composite of AgNWs and PDMS), forming

a conductive and stretchable layer.

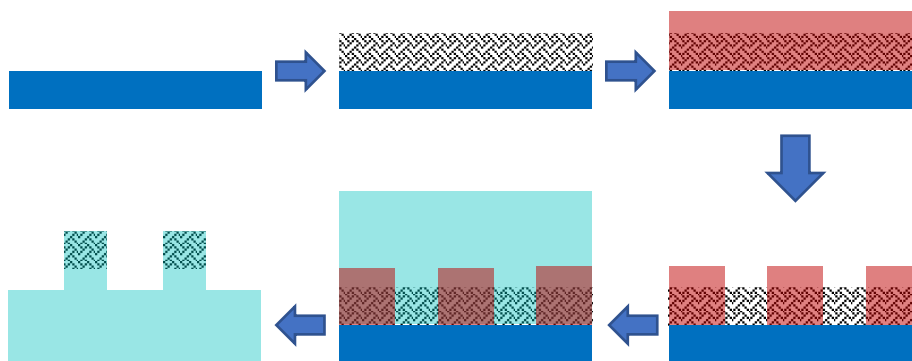


Figure 3.5 Schematic illustration of the AgNWs/PDMS electrodes fabrication by deposition and transferring method

Figure 3.6 shows the top-view image of AgNWs electrode after each fabrication process. While the liquid silicone is cast over the AgNWs networks, silicone would penetrate internal apertures inside the AgNWs networks, because of minimal viscosity and surface energy from liquid silicone. After crosslinking process of silicone, all silver nanowire networks would be embedded in crosslinked PDMS without obvious hollowness, exhibiting an effective transfer of silver nanowire film from silicon to silicone elastomers.

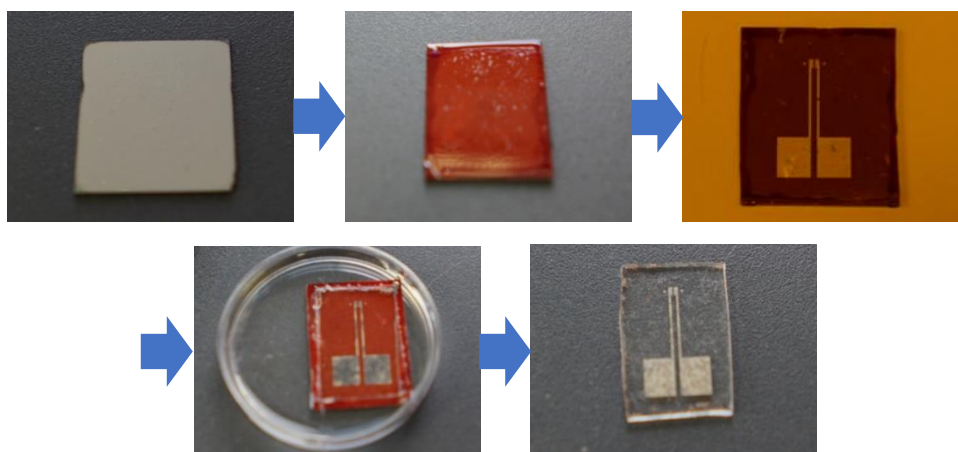


Figure 3.6 Photographs of AgNWs/PDMS electrode during the fabrication process.

Figure 3.9 presents the resistance variations with the changing of practical strains. It could be revealed that the resistance first grew from 3.32 to 8.66 Ω in linear when its strains enlarged up to 40%. After release of these strains, the resistance is incompletely recuperated and declined to 4.11 Ω if silicone elastomers are totally liberated.

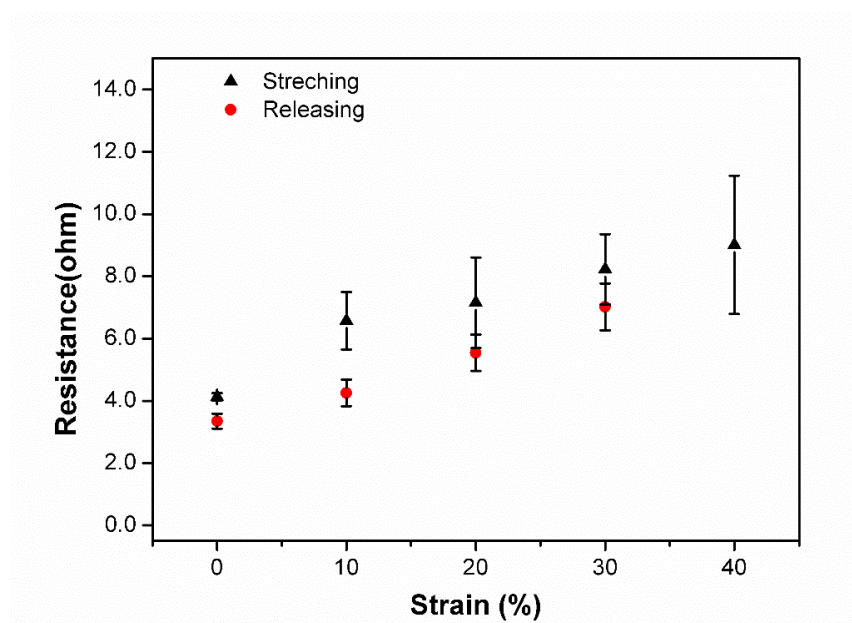


Figure 3.9 Resistances as the function of strain for the Ag NW/PDMS electrodes.

Extending/liberating cycles in strains span of 0–40% have been operated. The resistances exhibited no obvious variations after each extending cycle, while declined faintly after each liberating cycle. And a steady resistance would be realized through forth extending/liberating cycles and kept stable for more cycles in strains span of 0-40%.

3.4 Conclusion

Conducting polymer nanocomposites containing AgNWs fillers were

introduced to fabricate flexible electrodes. Two different methods to form the electrode with the AgNWs thin-film network after dipping deposition process are discussed in this chapter. The etching method was abandoned due to the unsettled residues. And the direct transferring method with traditional silicone technology applying a sacrificial layer could produce stretchable and transparent electrodes. Experimental studies demonstrated that the major causes which influence their electrical characteristics of silver nanowire nanocomposites would be AgNW concentrations and distribution state inside the silicone. When the Ag NWs were tightly connected by thermal annealing, their sheet resistance was decreased. With the good electrical, chemical, optical and mechanical properties of AgNWs/PDMS electrodes, they could be considered as an influential candidate for advanced flexible/ wearable applications.

Chapter 4 pH sensors based on AgNW/PAA hydrogel nanocomposite

4.1 Introduction

Hydrogel composite, accepted as fusion polymers, could be expressed as hydrating networks crosslinked with each other and inbedded with 1D/2D nanomaterials. In spite of natural advantages exhibited by the hydrogels, such as flexible physical, chemical and biological characteristics, excellent biocompatibilities and outstanding processibility, they still posses numerous shortages, e.g., weak mechanical strengths and poor thermal stabilities. These shortcomings would restrict their optimizations and efficient realizations in diverse applications [40-43]. Therefore, attentions for developments of hydrogel composites cooperated with nanomaterials are snowballing recently. Hydrogel composites could be optimized to posses excellent physical, chemical and electrical features.

Among various pH-sensitive hydrogels, PAA hydrogels have drawn giant attentions because of their excellent biocompatibilities as well as their outstanding film-formability. In addition, dense concentrations of carboxylic groups force they appropriate for modifying physically and chemically. Therefore, PAA hydrogels would promising to be employed in pH sensors [44, 45].

In this chapter, we discuss the adopted OMSL systems to fabricate Ag NW/PAA hydrogel composite to investigate the enhancement of sensor performance introduced by microstructures with the consideration to fully utilize the superior properties of the hydrogel composites in sensors.

4.2 AgNWs/PAA hydrogel composite for pH sensors

Stimuli-responsive or “smart” hydrogels are an outstanding polymer class, which facilitate sensor and actuator functions. Hydrogel networks reversible conversion of chemical energy into mechanical energy. For microsensor applications, the mechanical energy, in turn, can be converted into an electrical output signal.

4.2.1 Mechanism of AgNWs/PAA hydrogel composite-based pH sensor

Hydrogels swelling's transduction systems could be reliant with optical or mechanical techniques. Their functions through measuring variations within features of hydrogels networks, such as densities of crosslinking, volumes, or strain strengths induced from swelling/deswelling procedures [46-49]. Transducing in electrochemical would be mostly applied within biochemical sensing applications with outstanding reliability, expedited assessable regulations and the ease for the interfaces with complicated structures [50]. They provide probabilities of massive producing for low-cost flexible electronics to miniaturization and extensive purposes.

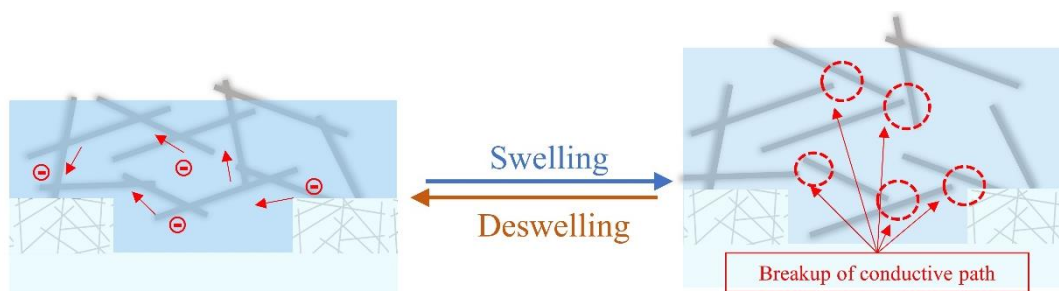


Figure 4.1 Schematic illustration of the pH response mechanism of AgNWs/PAA composites.

Within this work, a micropatterned resistive combined with ionic hydrogel, PAA, which shows a volume phase transition due to concentration changes of hydrogen ions. Therefore, they are suitable as sensitive sensor elements for pH detection. The network of PAA hydrogel would swell and shrink with the uptake and release of water from the applied pH stimulus, and this kind of change in volume would alter the spatial distribution of AgNWs in the hydrogel composite. The mechanism of transduction of AgNWs/PAA composites was shown in Figure 4.1. The pH value change would induce the volume change of PAA composite and then increase or decrease the distance between AgNWs in the composite due to the applied strain from volume changing. Therefore, the total resistance of the sensor will increase nonlinearly. Notably, the loss of contact among Ag NWs or breakup of conductive paths of AgNWs plays a significant role.

4.2.2 Patterning and testing of AgNWs/PAA hydrogel composite

The micropatterning process of AgNWs PAA composite with OMSL setup

is shown in Figure 4.2. And the microstructure fabrication process is as follows: photoinitiator (Irgacure 651) and crosslinker (MBA) was dissolved into AA with concentrations of 10wt.% and 0.5wt.%, respectively. Then the solution of Ag NWs dispersed into isopropanol solvent with 20 mg ml⁻¹ were added into the solution prepared. After that, the solutions were mixed with PVP powder with 10wt.% as the absorbent to keep AA monomer out of volatilization during to fabrication procedures. We spin-coated the solution prepared with 3000rpm with Keysight spin-coator to form a thin-film with around 2 um thickness. Then an own-developed OMSL setups are applied for the exposure procedure [51-55]. The pre-designed microstructures would be transferred to the own-defined image data and then it would be loaded onto a DMD chip for the production of serial exposure micropatterns.

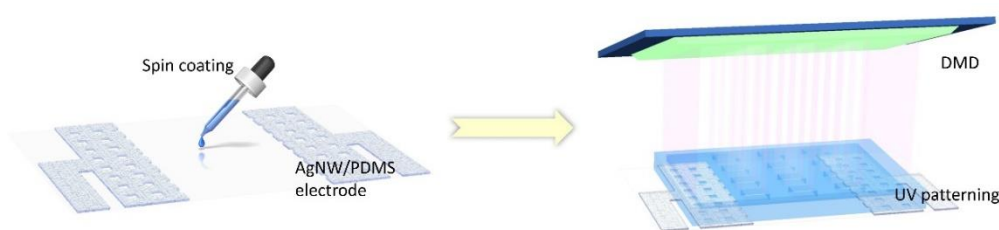


Figure 4.2 Schematic of micropatterning of AgNWs/PAA composites.

UV light sources (365nm) are applied in OMSL setups for AA monomer. The intensities of UV light sources for the microstructure's photopolymerization is 113.12 mW/cm². The whole photopolymerization time is around 10 to 30 seconds. The exposed microstructures of PAA are

developed through utilizing acetone and IPA, sequentially to remove the remanent uncurable chemicals including AA, Irgacure 651 and MBA and to dissolve the PVP in the composite due to the high solubility of IPA. For such kind of photopolymerizable hydrogel composites, the crosslinked PAA hydrogel would denote to the pH-sensitive properties, if AgNWs induce its conductivities. Mainly, the covalent crosslinked PAA hydrogels would play significant roles at reserving original conditions inside hydrogels structures, when hydrogen and ionizable bonds' dissociation/association is supporting energetic dissipations, therefore, improve elasticities of the hydrogel composites.

The mechanisms for photopolymerizations of PAA are decomposed to generate highly active radicals with UV lights. In this way, the monomer, AA, reacts with the active radicals due to the double bonds are also active for the reaction. And the PAA hydrogel can form in concise time as the radical polymerization is a fast way for hydrogel preparation.

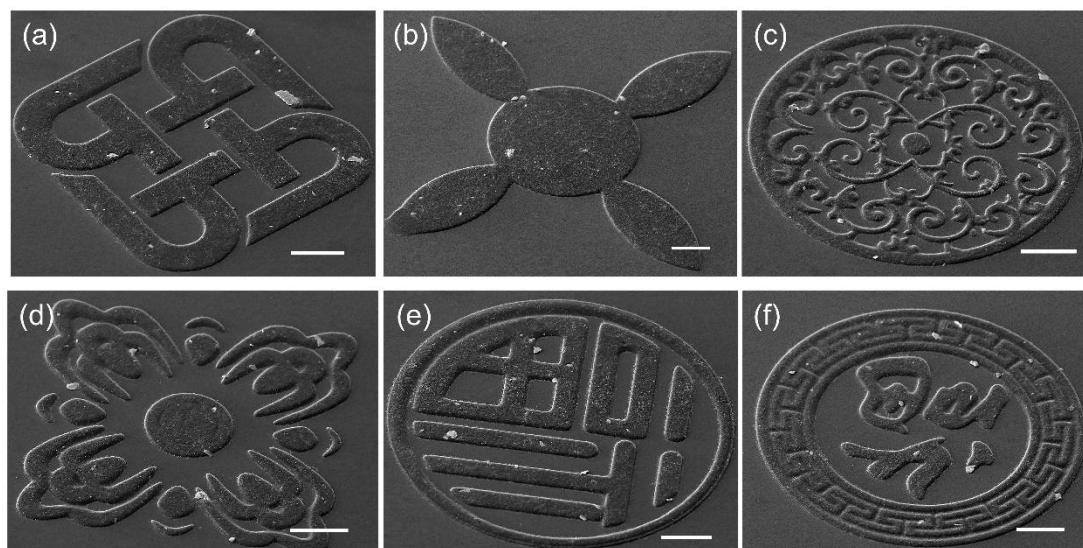


Figure 4.3 SEM images of micropatterned AgNWs/PAA composites. (a) PolyU log; (b) Clover; (c, d) Flower; (e, f) Character “Fu”. Scale bar: 100 μm .

The microstructures of AgNWs/ PAA nanocomposite were characterized through a 3D laser scanning confocal microscope (VK-X200, KEYENCE). It was a non-contact scan. The lens magnification applied here was 10x, 20x, 50x and 150x, respectively. Figure 4.3 show some microstructures with different line widths, ranging from 6 μm to 200 μm . Those microstructures include (a) PolyU logo ; (b) lucky clover; (c) and (d) different flowers; and (e) and (f) Chinese characters “fu”. They are all fabricated in between 10s and 20s. It can be seen from the pictures that the surface of all microstructures looks much smooth like without AgNWs due to the unmatched sizes of pattern and AgNW. The scale bar in the figure is 100 μm . Experimental results reveal that the lithography process can quickly pattern complex microstructures with different feature sizes. Because of the natural water-absorption features of hydrogels, the

connected points from thick microstructure will induce tiny swelling. In Figure 4.3, we can see the detailed SEM images of AgNWs/PAA nanocomposite. The scale bars for each picture are 50 μ m, 10 μ m, and 1 μ m. And here we can see the AgNWs which have homogenous distributions in the nanocomposite and also can see that the protrusion of AgNWs due to the large concentration. On the other hand, we can recognize that the micropatterning resolution-ratio for the AgNWs/PAA nanocomposite could reach 10 μ m in spite of copious protruding AgNWs.

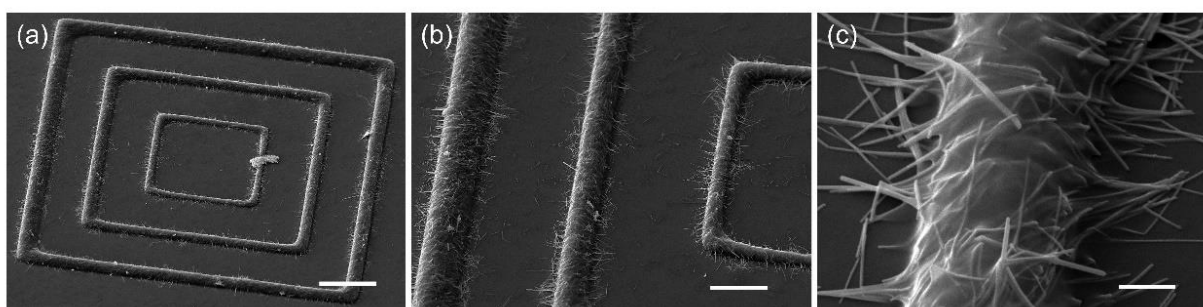


Figure 4.4 SEM images of micropatterned AgNWs/PAA composites. Scale bar are 50 μ m, 20 μ m and 5 μ m, respectively.

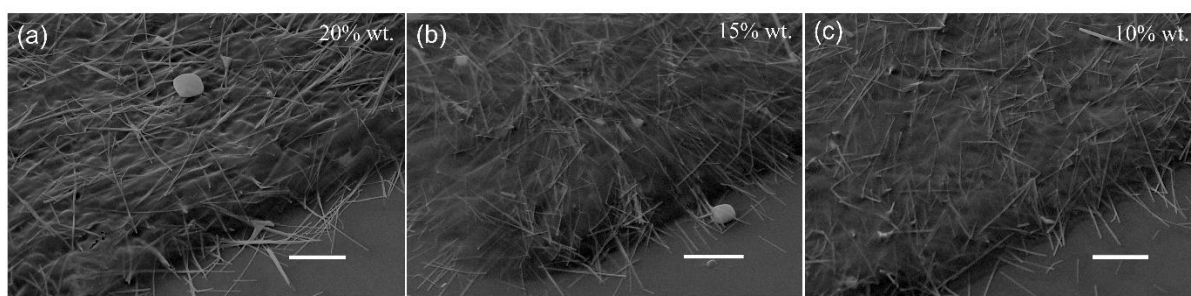


Figure 4.5 SEM images of AgNWs/PAA composites with the different concentrations of AgNWs: (a) 20wt.%, (b) 15wt.% and (c) 10wt.%. Scale bar: 10 μ m.

To estimate the effect from concentration on the performance of the pH sensor, we fabricated with three kinds of Ag NWs/ PAA composites with

10wt.%, 15wt.%, and 20wt.%, respectively. The SEM images for each hydrogel composites were shown in Figure 4.5. At the surface, the ratio of AgNWs in 20wt.% hydrogel composite is large than other two composites and also at the edges of hydrogel composites, the density of AgNWs of 20wt.% is greatest in comparison of three concentration.

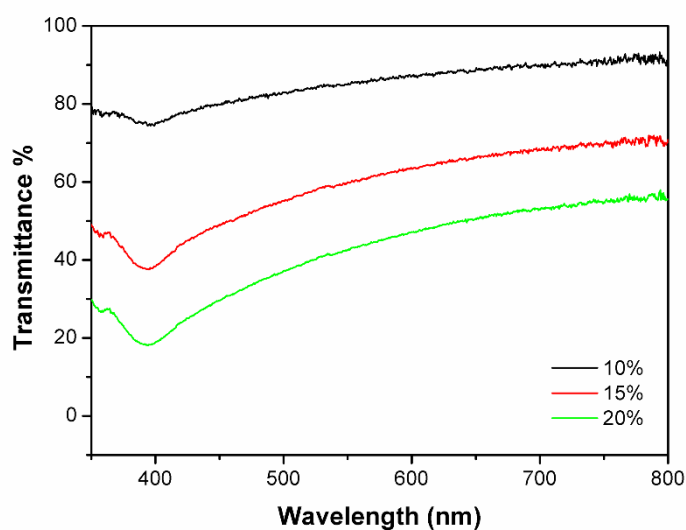


Figure 4.6 Transmittance spectra of the AgNWs/PAA composites with different concentrations 10, 15 and 20 wt.%, respectively.

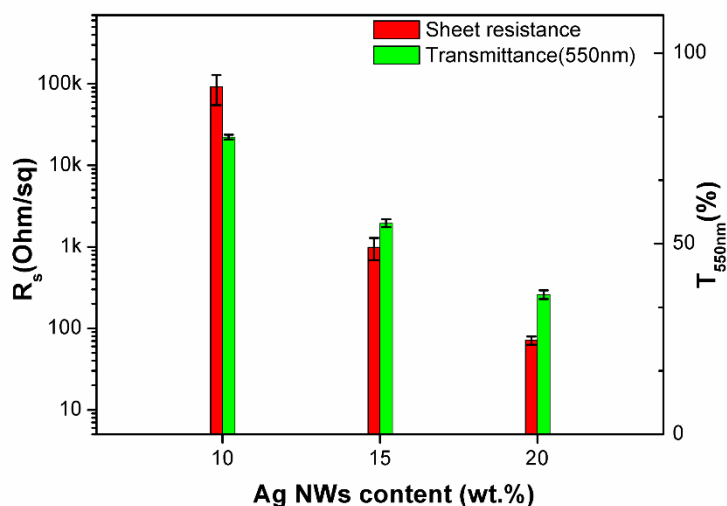


Figure 4.7 Statistics of sheet resistances and transmittances (550 nm) of the AgNWs/PAA composites with different concentrations 10, 15 and 20 wt.%, respectively.

Characterization about those three kinds of AgNWs/PAA composite was reported including conductivities, optical transmittances, and pH sensitivities, see in Figure 4.5. The concentration of AgNWs in the hydrogel composite would directly influence its optical transmittance in visible light which was shown in Figure 4.5.a. And here the deep at around 380 nm wavelength was observed due to absorption of AgNW in this waveband. We tested five more samples for each concentration and compared their sheet resistance and optical transmittance at 550nm wavelength. The results, in Figure 4.7, show that the sheet resistances have a nonlinear relationship with the Ag NWs concentration in the hydrogel nanocomposite. Besides, the optical transmittance at a 550nm decrease from 83.3% to 42.6% with the concentration of AgNWs increasing, approximately. Higher optical transmittance in visible light is one of the significant properties as the wearable electronics. In Figure 4.8, we characterized the pH responses of those three kinds of PAA/AgNWs composites. Similarly, each of the composites has a nonlinear (fitted with a 3rd polynomial) response from pH 2 to pH 7 and this result matched with the nonlinear changes of the hydrogel volume. And for 10wt.%, it has the largest sensitivities around pH 2 and pH 7 region, 39 k Ω /pH and 393.8 k Ω /pH respectively. For the hydrogel composite with 15wt.% concentration, it has 3.12 k Ω /pH and 92 k Ω /pH sensitivities for pH 2 and pH 7, respectively. And for the composite with 20wt.% concentration,

0.253 k Ω /pH and 56.2 k Ω /pH at pH 2 and pH 7. The response resistance of this kind of composite to pH is monotonically increasing so that the sensor which made from it could work regularly with a linear calibration even though the sensitivity of the composite is nonlinear.

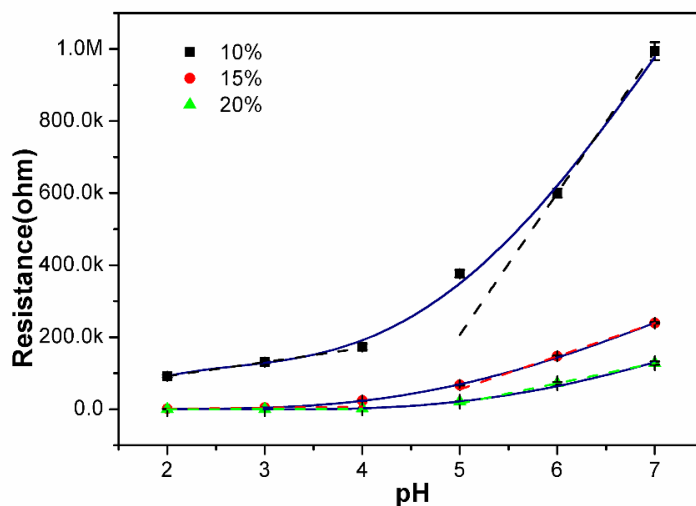


Figure 4.8 Resistance responses to pH (2-7) of the AgNWs/PAA composites of different concentrations with different concentrations 10, 15 and 20 wt.%, respectively.

Although the pH sensitivities for hydrogel composite with 10wt.% AgNWs content has the maximum pH sensitivities compared with others, the resistances for each pH value are too large which means the electric signals, especially the current signals, would be lower than one μ A when the applied commercial wearable electronic power supply (lower than 5V). Therefore, we choose the 20wt.% concentration PAA/AgNWs composite as the sensor element.

4.3 Fabrication and testing of the pH sensors based on AgNWs/PAA hydrogel composite

4.3.1 Fabrication of pH sensors based on AgNWs/PAA hydrogel

Figure 4.9 shows the schematic illustration of the flexible pH sensor with a microfluidic chip based on the AgNWs/ PAA hydrogel composite. The microfluidic chip was induced to collect the solution conveniently as well as to measure responses of the fabricated pH sensors precisely.

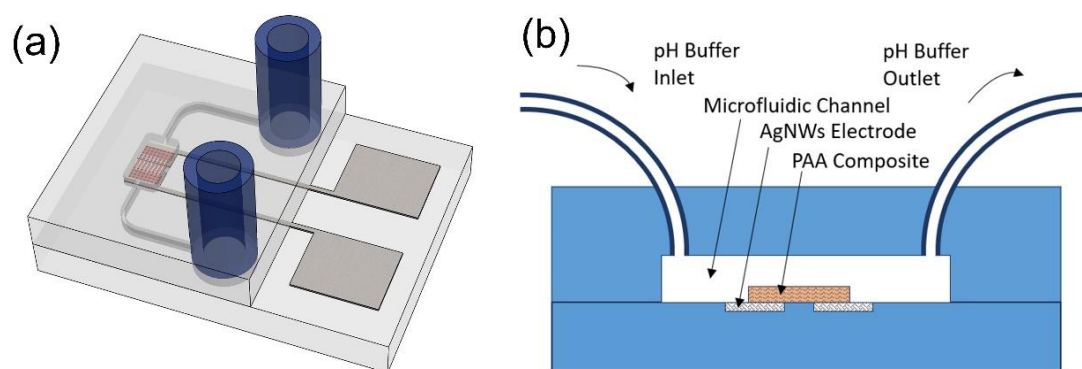


Figure 4.9 Schematic illustration (a) and cross-section (b) of an AgNWs/ hydrogel sensor integrated on a microfluidic chip.

The AA mixed solution with 20wt.% content of AgNWs was first dipped onto the prepared AgNWs/PDMS electrodes and spin-coated with 3000rpm to form a thin, responsive film between the designed a pair of electrodes. Afterward, an optical maskless photolithography technique would be used for micropatterning hydrogel composites into microgrid within the target electrodes with the alignment of the auxiliary cross near the electrodes. For the microfluidic chip, it was fabricated with the SU8 mold with a sink design adopted as the test area to contain both the sensing elements including AgNWs electrodes and PAA nanocomposite and

auxiliary cross. Figure 4.10 shows the images of manufactured flexible pH sensor with microchip based on the AgNWs/ PAA hydrogel composite. The testing image is shown in Figure 4.8.b. The inlet and outlet tubes were too heavy to be supported exclusively with the flexible microfluidic chip. And therefore, we adopted two book clips to sustain the sensor during testing.

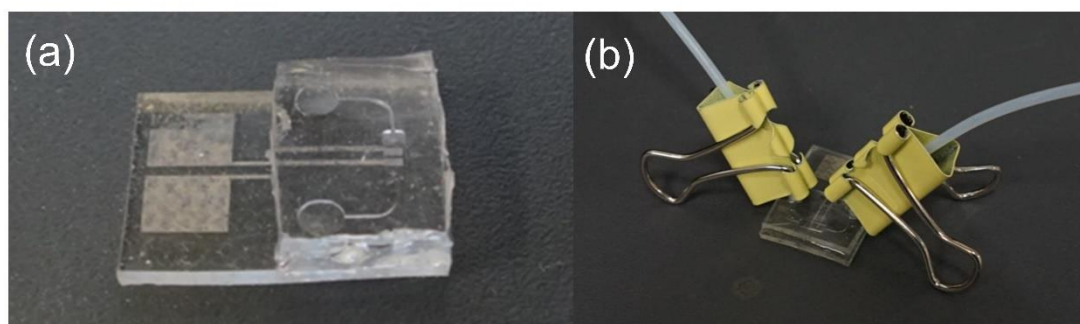


Figure 4.10 Photographs of an AgNWs/ hydrogel sensor-integrated microfluidic chip.

4.3.2 Testing results

Since 20wt.% Ag NW/PAA composite has the lowest standard deviation, it was selected to test its pH response in followed experiments. Figure 4.11 reveals the measured response from the sensor with a blank pattern (without microgrid pattern) to diverse pH liquid — the resistances of the pH sensor shift during the process of the pH increasing from 2 to 7. Figure 4.11b and 4.12b show the dynamic response of those sensors to pH changes. It shows that within same concentration of AgNW/PAA composite and same fabrication processes, the fabricated sensors would have almost same response at same pH solution. Each sensor immersed in pH solution for 5

minutes to ensure enough time for the swelling/deswelling process of the hydrogel composite.

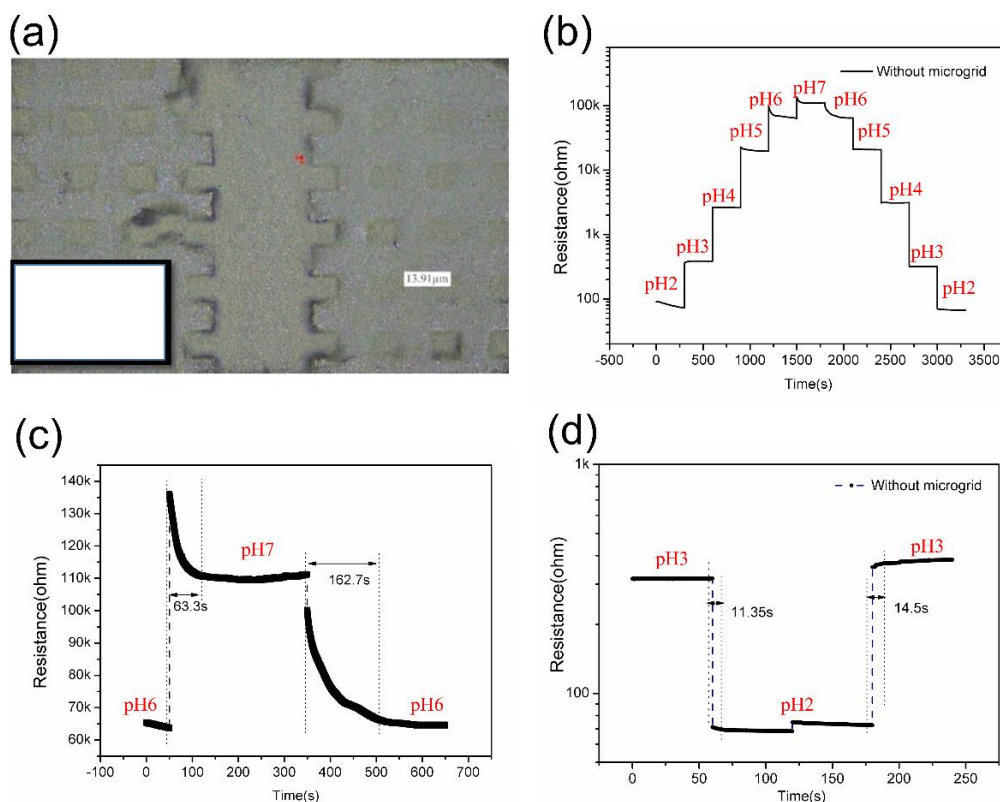


Figure 4.11 Dynamic measurements of 20wt.% sensors with blank micropattern. (a) the optical image of blank pattern on microelectrode, inset is the greyscale image; (b) the dynamic response to pH changing from 2 to 7 and vice-versa; (c,d) the response curve between pH 6 and 7, 2 and 3, respectively.

The dynamic response of 20 wt.% sensor without microgrid pattern to pH variations are presented in Figure 4.11. To realize the consistent measurement information, this PAA composite-sensor has been pre-soaked into deionized (DI) water before measurements. The tested response time of the sensor for increasing and decreasing pH processes are 100 and 130 s, respectively, which are comparable with other conductometric pH sensors.

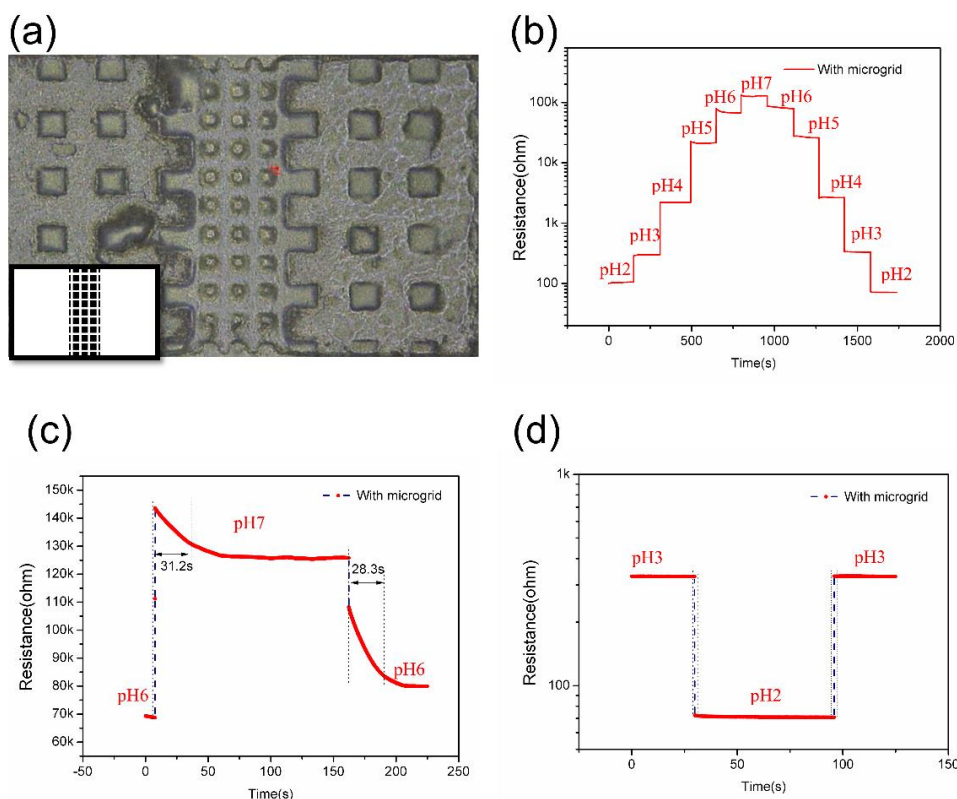


Figure 4.12 Dynamic measurements of 20wt.% sensors with microgrid pattern. (a) the optical image of microgrid pattern on microelectrode, inset is its greyscale image; (b) the dynamic response to pH changing from 2 to 7 and vice-versa; (c,d) the response curve between pH 6 and 7, 2 and 3, respectively.

Figure 4.11c and 4.12c test the response times of the sensors for increasing and decreasing from pH 6 to pH 7. The curves show that the sensor with microgrid structure has short response times 31.2s and 28.3s, respectively. Due to the nonlinearity of the swelling degree of the hydrogel, its responses including the equilibrium time and the changed volume are nonlinear, specifically, larger swelling degree under high pH would induce more response time. Figure 4.11d and 4.12d show the the response times of the sensors for increasing and decreasing from pH 2 to pH 3, the sensor with microgrid structure has a faster response around one tenth of that

without structure. And also, compared the responses between pH 6 and pH 7, there is also a great reduction of the response time.

Table 4.1 A comparison of pH sensor with the sensitivity response time and working rang with different sensor type.

Sensor type	Sensitivity	Response time	Working range	Years	Ref.
ISFET pH sensor	2.13 kΩ/pH	1-2 min	4-10	2016	[56]
Potentiometric pH sensor	55 mV/pH	<40 s	2-12	2018	[57]
Conductimetric pH sensor	100 Ω/pH	350 s	7-8	2011	[58]
Microcantilever pH sensor	60 nm/pH	30-75 s	4-10	2015	[59]
This work	56.2 kΩ/pH	<200 ms	2-7		

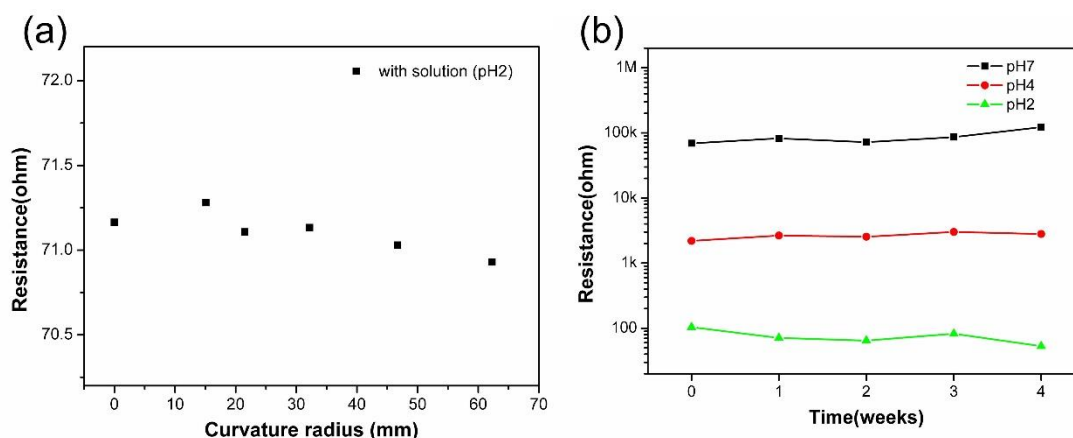


Figure 4.13 Resistance changes as a function of curvature radius in pH 2 (a) and drift of the pH sensor at various pH levels (b).

To trail the experiments about the mechanical flexibility of the pH sensor during curvature, its resistance immersed in pH 2 solution were measured with the function of curvature radius: curvature of up to 17 mm was used. The rate of resistance change, within diverse curvature radius, r , reveals roughly no variations after the curvature span applied, within the

maximum recorded resistance variation of only change of only $\sim 0.43\%$, as shown in Figure 4.13a. The results of the stability test show that during the first four weeks there is no significant change in the response resistance, as shown in Figure 4.13b.

4.4 Conclusion

In summary, this chapter introduces the pH sensing mechanism conductive PAA/ AgNWs hydrogel composites. We investigated the performance of the thin film from composites with different AgNWs contents. The optical maskless photopolymerization setup has been adopted to accurately micropattern the hydrogel composites within microgrid structures to improve the responding time.

Also, various intricate PAA/ AgNWs microstructures with different feature dimensions have been investigated to reveal the changeability of the processing techniques. Moreover, the microfluidic chip packaging process introduced to enhance the measurement environments. And the finally manufactured flexible pH sensor has high performance with a rapid response, high sensitivities, excellent flexibility, and outstanding stability. It should be noted that the proved micropatterning methods would activate interests in microengineering of PAA/AgNWs hydrogel composites as biosensing material.

Chapter 5 Discussion and future outlook

5.1 Discussion

Some limitations of the project are mentioned here for further improvements in the future. About the hydrogel PAA, even it performed a dramatic change in the pH range around 2-8 with determined pKa approximately at 5.5-6. It is not an optimal choice because this pKa is not so close to the pH of tissue living in reasonable condition (7.4), but it can be used as the model pH-sensitive hydrogel for developing a pH sensor.

Although the hydrogel sensor in this project did not work as expected to observe the pH changes in solutions, it showed the possibility to transduce physical changes of the hydrogel to electrical signals. Future improvements in packaging steps will help to solve the problems remaining in this project.

This project focuses on developing a pH-sensitive hydrogel based micro-sensor, especially for human applications to measure the pH change inside living tissue. The optimal pH for tissue working is properly 7.4 and may be reduced to around 6.6 due to diseases. So the hydrogel sensor was supposed to work and detect the change of pH in the range of 2-7. The pH-sensitive hydrogel sensor is based on the corporation of PAA/AgNWs composite into a piezoresistive sensor. The hydrogel was chosen

deliberately relied on its suitable properties and safety reasons. The hydrogel was individually investigated before incorporating into the piezoresistive sensor. To study the behaviors of the hydrogel in the micrometer scale, the hydrogel was synthesized inside a micro-fabricated cavity. The hydrogel can only perform its swelling and shrinking in one direction, allowing us to measure the changes in thickness of the hydrogel instead of the changes in the volume of the hydrogel in different pH buffers. A profilometer was utilized to determine the differences in thickness of the hydrogel responding to pH solutions.

Short measuring-time (less than equilibrium time) for the swelling of the hydrogel can cause a light shift on the curve of the behavior of the hydrogel to a higher range of pH. Besides, short measuring-time could not make the results for the difference in expansion degree of the different ratio in molar of PAA clear in these experiments. Moreover, experimental works showed that hydrogel PAA after hydration should be stored in a suitable pH buffer 2-3.

5.2 Future outlook

The work has demonstrated the excellent performance of the hydrogel composites PAA/AgNWs and the ability of a hydrogel sensor to transfer the swelling signal of the hydrogel to the electrical signal. Some suggestions can be made in the future. Firstly, it is necessary to fabricate a

custom made piezoresistive pressure sensor. A fabricated sensor with thinner cavity can allow synthesis of thinner hydrogel layer inside and thus a shorter response time of hydrogel. The thin hydrogel layer reaches the equilibrium status quicker and can help to reduce the hysteresis of the hydrogel behavior. Secondly, an improvement in the packaging of the hydrogel sensor should be figured out. The chemicals or adhesive components used in assembling of the hydrogel sensor should be waterproof and non-expansion in the aqueous working environment. This improvement is a decisive step to be able to record the signal from the sensor. Thirdly, since the experiments are conducted in room condition, effects of change of temperature and ambient pressure should be considered. We can make up a reference circuit to eliminate these changes of ambient temperature and pressure. Fourthly, other types of stimuli hydrogel can be interesting to study and incorporate to the piezoresistive pressure sensor such as ion-sensitive hydrogel, glucose-sensitive hydrogel, antigen-sensitive hydrogel, different kinds of the pH-sensitive hydrogel, etc. with pKa around seven which is closer to the pH of the living tissue should also be considered. Fifthly, a model for simulation should be built up based on the theory of the behavior of hydrogel to predict the changes of the hydrogel both in free and constraint expansion-shrinkage. Sixthly, as the hydrogel can be photo-sensitive, it can be photopatterned. A process to photopatterned should be attempted to produce the hydrogels in expected

shape and thickness with the purpose for further integrating into different transducers.

References

- [1] Yang, Yiran, and Wei Gao. Wearable and flexible electronics for continuous molecular monitoring. *Chemical Society Reviews* (2018).
- [2] Bandodkar, Amay J., Itthipon Jeerapan, and Joseph Wang. Wearable chemical sensors: Present challenges and future prospects. *ACS Sensors* 1.5 (2016): 464-482.
- [3] Windmiller, Joshua Ray, and Joseph Wang. Wearable electrochemical sensors and biosensors: a review. *Electroanalysis* 25.1 (2013): 29-46.
- [4] Asada, H. Harry, et al. Mobile monitoring with wearable photoplethysmographic biosensors. *IEEE engineering in medicine and biology magazine* 22.3 (2003): 28-40.
- [5] Pasche, Stéphanie, et al. Wearable biosensors for monitoring wound healing. *Advances in Science and Technology*. Vol. 57. Trans Tech Publications, 2008.
- [6] Ajami, Sima, and Fotooheh Teimouri. Features and application of wearable biosensors in medical care. *Journal of research in medical sciences: the official journal of Isfahan University of Medical Sciences* 20.12 (2015): 1208.

- [7] Gualandi, I., et al. Textile organic electrochemical transistors as a platform for wearable biosensors. *Scientific reports* 6 (2016): 33637.
- [8] Khan, Muhammad Imran, et al. A review on pH sensitive materials for sensors and detection methods. *Microsystem Technologies* 23.10 (2017): 4391-4404.
- [9] Yuqing, Miao, Chen Jianrong, and Fang Keming. New technology for the detection of pH. *Journal of biochemical and biophysical methods* 63.1 (2005): 1-9.
- [10] Herlem, Guillaume, et al. pH sensing at Pt electrode surfaces coated with linear polyethylenimine from anodic polymerization of ethylenediamine. *Journal of The Electrochemical Society* 148.11 (2001): E435-E438.
- [11] Talaie, Afshad. Conducting polymer based pH detector: A new outlook to pH sensing technology. *Polymer* 38.5 (1997): 1145-1150.
- [12] Deronzier, Alain, and Jean-Claude Moutet. Polypyrrole films containing metal complexes: syntheses and applications. *Coordination Chemistry Reviews* 147 (1996): 339-371.
- [13] Komura, T., et al. Charge-transporting properties of electropolymerized phenosafranin in aqueous media. *Journal of Electroanalytical Chemistry* 493.1-2 (2000): 84-92.
- [14] Jain, Mahaveer K., Qingyun Cai, and Craig A. Grimes. A wireless

- micro-sensor for simultaneous measurement of pH, temperature, and pressure. *Smart materials and structures* 10.2 (2001): 347.
- [15] Yuqing, Miao, Chen Jianrong, and Fang Keming. New technology for the detection of pH. *Journal of biochemical and biophysical methods* 63.1 (2005): 1-9.
- [16] Lakard, Boris, et al. Miniaturized pH biosensors based on electrochemically modified electrodes with biocompatible polymers. *Biosensors and Bioelectronics* 19.6 (2004): 595-606.
- [17] Wang, Xiaojuan, et al. Ratiometric pH-dot ANSors. *Analyst* 135.7 (2010): 1585-1591.
- [18] Bojinov, Vladimir B., Danail B. Simeonov, and Nikolai I. Georgiev. A novel blue fluorescent 4-(1, 2, 2, 6, 6-pentamethylpiperidin-4-yloxy)-1, 8-naphthalimide pH chemosensor based on photoinduced electron transfer. *Dyes and Pigments* 76.1 (2008): 41-46.
- [19] McNaughton, Brandon Howard, Jeffrey N. Anker, and Raoul Kopelman. Magnetic microdrill as a modulated fluorescent pH sensor. *Journal of Magnetism and Magnetic Materials* 293.1 (2005): 696-701.
- [20] Safavi, A., et al. CCD camera full range pH sensor array. *Talanta* 71.1 (2007): 498-501.
- [21] Khan, Muhammad Imran, and Fujiang Lin. Comparative analysis and design of harmonic aware low-power latches and flip-flops.

- Electron Devices and Solid-State Circuits (EDSSC), 2014 IEEE International Conference on. IEEE, 2014.
- [22] MICROSENS EPFL Switzerland (2007) Product specific data sheet—Ion sensitive field effect transistors (ISFETS). MICROSENS EPFL Innovation Park Building, Lausanne, Switzerland.
- [23] Kumar, Sachin, et al. Soil pH Sensing Techniques and Technologies A Review. *International Journal of Advanced Research in Electrical, Electronics and Instrumentation Engineering* 4.5 (2015): 4452-4456.
- [24] Karyakin, Arkady A., et al. Potentiometric biosensors based on polyaniline semiconductor films. *Sensors and Actuators B: Chemical* 33.1-3 (1996): 34-38.
- [25] Lakard, Boris, et al. Miniaturized pH biosensors based on electrochemically modified electrodes with biocompatible polymers. *Biosensors and Bioelectronics* 19.6 (2004): 595-606.
- [26] Lakard, Boris, et al. Potentiometric pH sensors based on electrodeposited polymers. *Polymer* 46.26 (2005): 12233-12239.
- [27] Kang, Tian-Fang, et al. Potentiometric pH sensors based on chemically modified electrodes with electropolymerized metal-tetraaminophthalocyanine. *Talanta* 45.2 (1997): 291-296.
- [28] Lakard, Boris, et al. Potentiometric miniaturized pH sensors based

- on polypyrrole films. *Sensors and Actuators B: Chemical* 122.1 (2007): 101-108.
- [29] Richter, Andreas, et al. Review on hydrogel-based pH sensors and microsensors. *Sensors* 8.1 (2008): 561-581.
- [30] van der Linden, Heiko J., et al. Stimulus-sensitive hydrogels and their applications in chemical (micro) analysis. *Analyst* 128.4 (2003): 325-331.
- [31] Tanaka, Toyochi. Collapse of gels and the critical endpoint. *Physical Review Letters* 40.12 (1978): 820.
- [32] Arndt, Karl-Fr, et al. High response smart gels: synthesis and application. *Macromolecular Symposia*. Vol. 207. No. 1. Weinheim: WILEY-VCH Verlag, 2004.
- [33] Siegel, Ronald A., and Bruce A. Firestone. pH-dependent equilibrium swelling properties of hydrophobic polyelectrolyte copolymer gels. *Macromolecules* 21.11 (1988): 3254-3259.
- [34] Seitz, W. Rudolf. New directions in fiber optic chemical sensors: sensors based on polymer swelling. *Journal of molecular structure* 292 (1993): 105-113.
- [35] Liu, Xiaomei, et al. Demonstration of etched cladding fiber Bragg grating-based sensors with hydrogel coating. *Sensors and Actuators B: Chemical* 96.1-2 (2003): 468-472.
- [36] Richter, Andreas, et al. Characterization of a microgravimetric

- sensor based on pH sensitive hydrogels. *Sensors and Actuators B: Chemical* 99.2-3 (2004): 579-585.
- [37] Suzuki, A., and H. Suzuki. Hysteretic behavior and irreversibility of polymer gels by pH change. *The Journal of chemical physics* 103.11 (1995): 4706-4710.
- [38] Harmon, Marianne E., Dirk Kuckling, and Curtis W. Frank. Photo-cross-linkable PNIPAAm copolymers. 2. Effects of constraint on temperature and pH-responsive hydrogel layers. *Macromolecules* 36.1 (2003): 162-172.
- [39] Richter, Andreas, et al. Influence of volume phase transition phenomena on the behavior of hydrogel-based valves. *Sensors and Actuators B: Chemical* 99.2-3 (2004): 451-458.
- [40] Bhattacharya, Sanchita, et al. Temperature-, pH-, and magnetic-field-sensitive hybrid microgels. *Small* 3.4 (2007): 650-657.
- [41] Yuk, Hyunwoo, et al. Skin-inspired hydrogel–elastomer hybrids with robust interfaces and functional microstructures. *Nature communications* 7 (2016): 12028.
- [42] Zhang, Yu Shrike, and Ali Khademhosseini. Advances in engineering hydrogels. *Science* 356.6337 (2017): eaaf3627.
- [43] Pu, Xiong, et al. Ulstretchable, transparent triboelectric nanogenerator as electronic skin for biomechanical energy harvesting and tactile sensing. *Science advances* 3.5 (2017):

e1700015.

- [44] Liu, Yaqing, et al. Nature-inspired structural materials for flexible electronic devices. *Chemical reviews* 117.20 (2017): 12893-12941.
- [45] Tang, Jingda, et al. Fatigue fracture of hydrogels. *Extreme Mechanics Letters* 10 (2017): 24-31.
- [47] Hu, Liangbing, et al. Scalable coating and properties of transparent, flexible, silver nanowire electrodes. *ACS nano* 4.5 (2010): 2955-2963.
- [48] Xu, Feng, and Yong Zhu. Highly conductive and stretchable silver nanowire conductors. *Advanced materials* 24.37 (2012): 5117-5122.
- [49] Amjadi, Morteza, et al. Highly stretchable and sensitive strain sensor based on silver nanowire–elastomer nanocomposite. *ACS nano* 8.5 (2014): 5154-5163.
- [50] Gaynor, Whitney, et al. Smooth nanowire/polymer composite transparent electrodes. *Advanced Materials* 23.26 (2011): 2905-2910.
- [51] Van De Groep, Jorik, Pierpaolo Spinelli, and Albert Polman. Transparent conducting silver nanowire networks. *Nano letters* 12.6 (2012): 3138-3144.
- [52] Lim, Guh-Hwan, et al. Curving silver nanowires using liquid droplets for highly stretchable and durable percolation networks. *Nanoscale* 9.26 (2017): 8938-8944.

- [53] Finn, David J., Mustafa Lotya, and Jonathan N. Coleman. Inkjet printing of silver nanowire networks. *ACS applied materials & interfaces* 7.17 (2015): 9254-9261.
- [54] Yin, Ming-Jie, et al. Rapid 3D patterning of poly (acrylic acid) ionic hydrogel for miniature pH sensors. *Advanced materials* 28.7 (2016): 1394-1399.
- [55] Yin, Ming-jie, et al. Micropatterned Elastic Gold-Nanowire/Polyacrylamide Hydrogel composites for Wearable Pressure Sensors. *Advanced Materials Technologies* (2018): 1800051.
- [56] Li, Yu-Ren, et al. "High-Sensitivity Extended-Gate Field-Effect Transistors as Ph Sensors with Oxygen-Modified Reduced Graphene Oxide Films Coated on Different Reverse-Pyramid Silicon Structures as Sensing Heads." *Japanese Journal of Applied Physics* 55 4S (2016).
- [57] Tanumihardja, E., W. Olthuis, and A. van den Berg. "Ruthenium Oxide Nanorods as Potentiometric Ph Sensor for Organs-on-Chip Purposes." *Sensors (Basel)* 18 9 (2018).
- [58] Lei, Nan, et al. "Simple Graphene Chemiresistors as Ph Sensors: Fabrication and Characterization." *Measurement Science and Technology* 22 10 (2011).
- [59] Jun, Li, et al. "A Micro-Machined Optical Fiber Cantilever as a

Miniaturized Ph Sensor." IEEE Sensors Journal 15 12 (2015):
7221-28.